Transportation Science

Publication details, including instructions for authors and subscription information:
http://pubsonline.informs.org

Designing a Reliable and Dynamic Multimodal Transportation Network for Biofuel Supply Chains

Mohammad Marufuzzaman, Sandra Duni Ekşioğlu

To cite this article:
Mohammad Marufuzzaman, Sandra Duni Ekşioğlu (2017) Designing a Reliable and Dynamic Multimodal Transportation Network for Biofuel Supply Chains. Transportation Science 51(2):494-517. https://doi.org/10.1287/trsc.2015.0632

http://pubsonline.informs.org/journal/trsc/

TRANSPORTATION SCIENCE
Vol. 51, No. 2, May 2017, pp. 494–517
ISSN 0041-1655 (print), ISSN 1526-5447 (online)

Designing a Reliable and Dynamic Multimodal Transportation Network for Biofuel Supply Chains

Mohammad Marufuzzaman,[a] **Sandra Duni Ekşioğlu**[b]

[a] Department of Industrial and Systems Engineering, Mississippi State University, Starkville, Mississippi 39762; [b] Department of Industrial Engineering, Clemson University, Clemson, South Carolina 29634

Contact: maruf@ise.msstate.edu (MM); seksiog@clemson.edu (SDE)

Received: May 19, 2014
Revised: March 19, 2015
Accepted: May 16, 2015
Published Online in Articles in Advance: May 13, 2016

https://doi.org/10.1287/trsc.2015.0632

Abstract. This paper presents a cost-efficient and reliable supply chain network design model for biomass to be delivered to biofuel plants. Biomass is bulky, so transportation modes such as rail and barge can be used to deliver this product. For this reason, this study focuses on multimodal supply chain designs for biofuel. Biomass supply is highly seasonal, but the high production seasons for biomass in the Southeast United States often coincide with or are followed by hurricanes, and drought seasons, both of which impact transportation. The dynamic multimodel transportation network design model this paper presents enables this supply chain to cope with biomass supply fluctuations and to hedge against natural disasters. The mixed-integer nonlinear programming model proposed is an $\mathcal{NP}$-hard problem, and we develop an accelerated Benders decomposition algorithm and a hybrid rolling horizon algorithm to solve this problem. We tested the performance of the algorithm on a case study using data from the Southeast United States. The numerical experiments show that this proposed algorithm can solve large-scale problem instances to a near optimal solution in a reasonable time. Numerical analyses indicate that, under normal conditions, the minimum cost model outperforms the reliable models. However, under disaster scenarios, the minimum cost model is 2.65% to 9.20% more expensive than the reliable and static model and 6.28% to 17.73% more expensive than the reliable and dynamic model. Thus, the reliable and dynamic multimodal network design decisions can aid biofuel supply chain management decisions, especially when considering the potential impacts of natural disasters.

Funding: This work is supported partially by the National Science Foundation [Grant CMMI 1052671], and the Mississippi Department of Transportation [Grant SPR-1(66)/106461-179000].

Keywords: biofuel supply chain network • dynamic multimodal transportation model • Benders decomposition • rolling horizon heuristic

1. Introduction

Production of biofuels is expected to increase in the near future because of the requirements set by the Renewable Fuel Standards (RFS) (U.S. Environmental Protection Agency 2007). Based on these requirements, 36 billion gallons a year (BGY) of biofuels should be produced by 2022. These standards cap corn-ethanol production to 15 BGY, and they require that at least 16 BGY of cellulosic biofuels be produced. In 2013, 1.3 billion gallons (BG) of biodiesel (U.S. Energy Information Administration 2013a) and 13.3 BG of ethanol (Renewable Fuels Association 2013) were produced and production of cellulosic biofuels is expected to continue to increase. Investors will need tools to support their supply chain design and management decisions, so the goal of this paper is to build models of cellulosic biofuel supply chains that ensure efficient and reliable performance.

The efficiency and reliability of the supply chain are crucial aspects of the biofuel industry. Ensuring that these supply chains are cost-efficient is challenging because of the physical characteristics of the raw material used to produce these biomass fuels. Biomass is bulky and difficult to transport; its supply is seasonal and uncertain; and biomass is widely dispersed geographically. For these reasons, collection and transportation costs are high. Modes like rail and barge can be used to deliver biomass to reduce transportation costs. These modes are typically used for long-haul and high-volume shipments of other bulk products, such as corn, soybeans, and other large harvest crops. When barge is used, the supply chain becomes vulnerable to unexpected natural disasters, such as floods, hurricanes, and droughts,—which interrupt the supply chain's regular operations. Therefore, designing reliable supply chains to hedge against risks from unexpected natural disasters is important. The model proposed here is an integer program that minimizes costs of supply chain activities and hedges against risks from unexpected natural disasters. This model will serve managers of biofuel plants who face supply chain design and management decisions.

One of the motivations for this work is the powerful impact that catastrophic events have on transportation infrastructure and logistics management. For example, natural disasters like Hurricane Katrina in 2005 (National Oceanic and Atmospheric Administration 2005), the earthquakes in China and Haiti in 2008 and 2009, respectively (Gill 2010), and human-caused disasters, such as the 2003 U.S. Northeast blackout (Pacific Northwest National Laboratory 2013) and the 2010 Gulf of Mexico oil spill (Polson 2011), devastated transportation systems and consequently interrupted logistics and supply chain activities. Furthermore, the timing of potential disruptions due to hurricanes and floods corresponds with the harvest season for biomass. For example, the harvest season for corn stover—typically early September until late November—coincides with the hurricane season in the Southeast and is followed by droughts of agricultural waterways. Historical records indicate that the Southeast hurricane season starts in mid-August and continues until the end of October (see Figure 1(a)) (State Climate Office at North Carolina 2012). Hurricanes also impact agricultural waterways shipments of biomass to the Gulf of Mexico and shipments of stover to and from the North Carolina and South Carolina Atlantic coastlines. Droughts along the Mississippi River and other agricultural waterways typically happen during the winter because of the impacts moisture and cold weather have in the Midwest (see Figure 1(b)) (U.S. Drought Monitor 2013b). Other disruptions, such as flooding of the Mississippi River and its tributaries (see Table A.1 in the appendix), impacts biofuel supply chain operations. Thus, biomass seasonality, coupled with transportation uncertainty due to disruptions, impacts supply chain performance. To handle these uncertainties efficiently, managers need to adjust their short-term and midterm supply chain decisions dynamically.

To manage the supply chain and cope with facility disruptions, managers need decision-support tools. These tools should capture the seasonal nature of biomass supply, use the proper transportation modes for biomass transportation, and rely on existing practices used to manage agricultural products' supply chains. The model proposed in this paper accounts for these important observations. We present a multimodal transportation network to design the inbound supply chain of biofuel facilities. Multimodal transportation network models are typically used to design supply chains for bulk products, such as corn and other agricultural products. The first hub in the network serves as a shipment consolidation point, and the second hub is a deconsolidation point. Rail and barge transport biomass between hubs since these modes are typically used for high-volume, long-haul transportation of bulk products. The model proposed is dynamic because it identifies when to open new biorefineries and in which season to use, or discontinue using, a multimodal facility. The model also determines a transportation schedule for shipments between facilities and identifies a production schedule and inventory levels.

To optimize costs in this supply chain, the model allows facilities the flexibility of using different modes of transportation—thus different multimodal facilities—in different seasons. This practice is followed by many companies that deliver corn and grains by barge from the Midwest to the Gulf of Mexico. For example, because of the Mississippi River drought during the winter, companies use rail or truck instead of barge. Another practice is to maintain inventories and delay biomass delivery. Although these practices reduce the impact that potential disruptions may have on the supply chain, transportation or inventory costs will increase because some modes of transportation are more expensive or because carrying inventory

Figure 1. (a) The Total Number of Stormy Days in North Carolina from 1851 to 2012 (State Climate Office at North Carolina 2012), and (b) Contiguous U.S. Drought Areas (in %) (U.S. Drought Monitor 2013b)

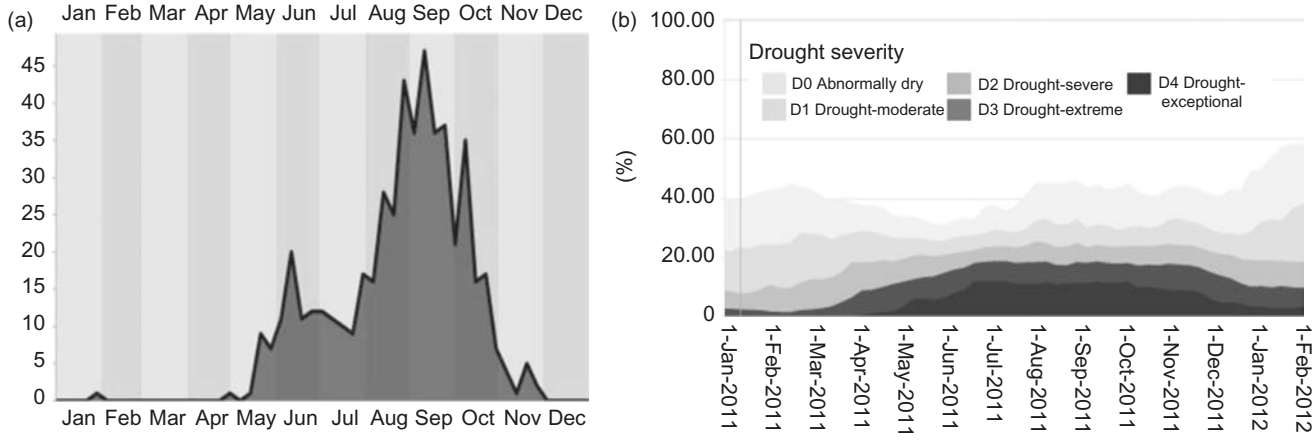

increases costs. Clearly, making these decisions is not easy since they are impacted by biomass availability, inventory holding costs, transportation costs, and other concerns. Models like the one proposed in this paper are useful for decision makers since they aid in making supply chain decisions that minimize the overall system costs. The model proposed here minimizes costs under normal and disruption scenarios.

The model proposed is an extension of the classical fixed charge network design problem, which is known to be an $\mathcal{NP}$-hard problem (Magnanti and Wong 1981). Therefore, solving large instances of this supply chain problem is a challenging task. For this reason, we develop and implement two algorithms: a rolling horizon (RH)-based heuristic and an enhanced Benders decomposition algorithm. Numerical experiments confirm that both algorithms efficiently solve midsized problem instances. For large-scale problems, an algorithm that integrates the rolling horizon heuristic and the accelerated Benders decomposition algorithm provides near optimal solutions by avoiding the stand alone algorithms prohibitively long running times. We implement these algorithms using data from a case study of the Southeast United States. The results from solving the case study provide detailed periodic production and transportation plans that capture feedstock seasonality and hedge against risk due to unexpected natural disasters. In summary, the key contributions of this paper are (a) the development of a new, dynamic, integrated reliable hub location and network design problem—the corresponding mixed-integer linear programming (MILP) formulation presented proposes a supply chain design that minimize costs and mitigates risks due to disruptions and biomass supply seasonality; (b) the development of a Benders-based rolling horizon heuristic, which provides high-quality solutions for large problem instances in a reasonable amount of time; and (c) the development of a real-life case study based on data from the southeast region of the United States.

The remainder of this paper is organized as follows: A review of the literature is given in Section 2; Section 3 formulates the mathematical model; Section 4 introduces the solution algorithms; Section 5 presents numerical results and draws managerial insights; and finally Section 6 concludes this paper.

2. Literature Review

Since the mid-2000s, research in biofuel supply chains has focused on minimizing the total system costs. These studies develop integrated biofuel supply chain networks to deliver biofuel at a competitive price to the end users. To achieve this goal, studies such as Zamboni, Shah, and Bezzo (2009) and Eksioglu et al. (2010) develop deterministic models optimizing the total plant location and transportation costs in biofuel supply chain networks. These works are extended by Eksioglu et al. (2009), Kang et al. (2010), Huang, Chen, and Fan (2010), An, Wilhelm, and Searcy (2011), Eksioglu et al. (2013); and Xie, Huang, and Eksioglu (2014) to capture system dynamics better by considering multiple periods of optimization frameworks. Xie and Ouyang (2013) develop a mixed-integer programming model for a dynamic, multitype, facility colocation problem, which, during a fixed planning horizon, minimizes the total costs from facility construction, capacity expansion, and transportation. The authors use an accelerated Benders decomposition algorithm to solve large-sized problem instances. To capture system uncertainties, Kim, Realff, and Lee (2011), Chen and Fan (2012); and Huang, Fan, and Chen (2014) develop stochastic models to aid with the design and management of biofuel supply chain networks. One of the key assumptions of the above mentioned literature is that facilities—some of which are multimodal transportation facilities—are robust and never fail. However, unexpected disruptions at transportation facilities have been observed on multiple occasions (Mouawad 2005; Credeur 2011; Polson 2011). These facts highlight the need to address the potential risk of facility failures in the process of designing and managing biofuel supply chain networks.

The practice with other agricultural products indicates that the inbound supply chain systems for biorefineries should rely on using multiple modes of transportation. Research by Eksioglu et al. (2010) is one of the first works that evaluates the impact of accessibility to a multimodal transportation network on the biofuel supply chain performance. Most recently, Xie, Huang, and Eksioglu (2014) extend this work by developing a fully integrated multimodal transportation system for the cellulosic biofuel supply chain network. Both these models consider biomass supply fluctuations due to seasonality. The model proposed here is closely related to these studies. However, unlike these works, which assume that the transportation system is reliable and never fails, the model proposed here considers the impact of disruptions of multimodal hubs in the biofuel supply chain performance. Other studies that analyze the impacts of multimodal transportation hubs in the supply chain network design decisions are Oosterhuis, Molleman, and Vaart (2005), Melo, Nickel, and Saldanha da Gama (2005); and Hinojosa et al. (2008).

Although many researchers have focused on hub location models, only two papers in the literature specifically study the dynamic hub location problem. Campbell (1990) develops a continuous approximation model to help transportation terminals handle an increasing regional demand for their services. Contreras, Cordeau, and Laporte (2011) develop a dynamic, uncapacitated, hub location problem that minimizes the total system cost over a finite planning horizon. The

model proposed in this paper is an extension of the paper by Contreras, Cordeau, and Laporte (2011). Our work differs because it considers hub disruptions as part of a dynamic multimodal transportation network design problem. Additionally, we propose customized algorithms, extensions of the Benders decomposition algorithm (Benders 1962) and the rolling horizon heuristic (Kostina et al. 2011), and provide a real-world case study to show the efficiency and efficacy of the proposed models and solution algorithms.

Reliability issues in supply chain design are a topic of interest for many researchers. Peng et al. (2011) state that even a carefully constructed supply chain network can be severely damaged if, during the design phase, managers fail to consider potential disruptions. Daskin (1982, 1983) first considers facility unavailability in a maximal covering location problem. This work is extended by Drezner (1987) by developing models for reliable p-median location problems. Snyder and Daskin (2005) propose models for reliable uncapacitated fixed-charge location problems (UFLP) and the p-median problem where facility disruptions occur randomly with identical probability. Cui, Ouyang, and Shen (2010), Li and Ouyang (2010), Shen, Zhan, and Zhang (2011); and Li, Zeng, and Savachkin (2013) extend existing models by relaxing the uniform disruption probability assumption introduced by Snyder and Daskin (2005). A brief overview of the reliability facility location models can be found from a study by Snyder et al. (2006).

A major stream of research has already been conducted on reliable facility location models. However, the model, which considers reliable multimodal transportation network design problems, is scarce. To our knowledge, the model proposed by An, Zhang, and Zeng (2015) is the only study that addresses reliability issues for the single- and multiple-allocation hub-and-spoke network design problems. The authors consider disruptions at transportation hubs where the risk of hubs becoming unavailable is mitigated by identifying backup hubs and alternative transportation routes. This work is closely related to the work presented here, but the model we propose considers a multimodal transportation network design model that mitigates risk by deciding at the planning stage what hub to use, or discontinue using, during different seasons of the year. Therefore, our model proposes a proactive, not a reactive, approach to manage the supply chain.

Despite all these efforts, little work has been done to address the impact of disruptions to the biofuel supply chain network design and management. Li et al. (2011) propose one discrete and one continuous model to design reliable bioethanol supply chain networks. They use numerical analysis to evaluate the impact of disruptions on optimal refinery deployment decisions. Wang and Ouyang (2013) propose a game-theoretical-based, continuous approximation model to locate biorefineries under spatial competition and facility disruption risks. These studies only consider failure risks at biorefineries. These studies do not focus on evaluating the impact that disruptions of intermediate transportation facilities have on the biofuel supply chain performance. The model we propose fills this gap that exists in the current literature.

3. Problem Description and Model Formulation

This section presents a mathematical model for a multiperiod biofuel supply chain network design and management problem. The model considers potential facility disruptions and responds by dynamically identifying the multimodal facilities to use, or discontinue using, in each period to optimize systemwide costs. Section 3.1 provides a mixed-integer nonlinear programming (MINLP) formulation of the problem, referred to as **[DR]**. Section 3.2 provides an MILP formulation, which is easier to solve with commercial software and the algorithms we propose in Section 4.

3.1. Nonlinear Problem Formulation

Let $\mathcal{G}(\mathcal{N}, \mathcal{A})$ denote the supply chain network for the problem presented in this paper. Figure 2 gives an

Figure 2. Network Configuration of a Biofuel Supply Chain

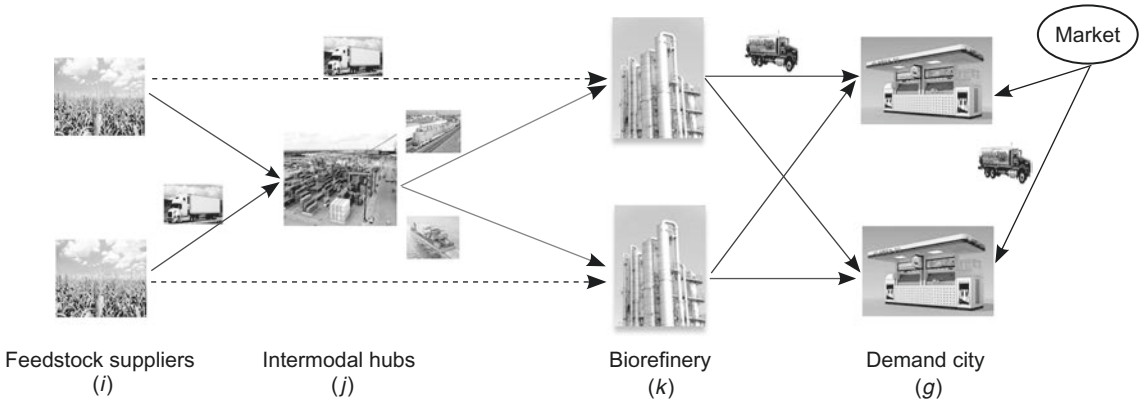

example of the network structure for a biofuel supply chain that consists of two suppliers, one multimodal facility, two biorefineries, and two markets. The set of nodes in $\mathcal{G}(\mathcal{N}, \mathcal{A})$, denoted by $\mathcal{N}$, consists of the set of suppliers $\mathcal{I}$, the set of candidate multimodal facility locations $\mathcal{J}$, the set of candidate biofuel plant locations $\mathcal{K}$, and the set of markets $\mathcal{G}$. Each supplier $i \in \mathcal{I}$ produces s_{it} units of biomass in time period $t \in \mathcal{T}$. Each market $g \in \mathcal{G}$ demands b_{gt} gallons of biofuel in period t. This formulation assumes that a substitute product in the market can be used to satisfy the demand for biofuel. The market price for the substitute product is denoted by π_{gt}. This price, which is exogenously determined, represents the penalty per unit of unsatisfied demand. This penalty also serves as a threshold of the biofuel's unit delivery cost using the proposed system. That means, if the unit cost of delivering biofuel to markets through this supply chain exceeds the threshold, then demand will be satisfied by the substitute product.

For nodes $j \in \mathcal{J}$, Ψ_{ljt} denotes the fixed cost of using hub j of capacity $l \in \mathcal{L}^h$ at the beginning of time period t. We assume that the hubs are already located at a given location $j \in \mathcal{J}$ and the fixed cost of using the hub (e.g., build additional sidings (track and turnout), purchasing forklifts) represents the additional infrastructure that is required to connect a biofuel plant to this hub. Our motivation here comes from real-life applications. Many large-scale production facilities have direct access to rail and barge transportation. We denote η_{ljt} as the recovery gain associated with discontinued use of the hub. Ψ_{lk} is the fixed cost of locating a biofuel plant of capacity $l \in \mathcal{L}^b$ in location $k \in \mathcal{K}$. Multimodal facilities serve as shipment consolidation points. We assume that every biofuel plant is colocated with a multimodal facility and the capacity of the multimodal facility is assumed to be equal of the biorefinery. We further assume that the transportation costs between the biorefinery and the multimodal facility are negligible. This assumption is derived from the fact that many large-scale production facilities have direct access to shipping by rail and barge.

The set of arcs, denoted by $\mathcal{A}$, consists of four disjoint subsets, $\mathcal{A}^1, \ldots, \mathcal{A}^4$. Let c_{ijt} for $(i, j) \in \mathcal{A}$ denote the variable unit cost of moving products along these arcs in time period t. Set $\mathcal{A}^1$ consists of the arcs joining suppliers with multimodal facilities; set $\mathcal{A}^2$ consists of arcs connecting multimodal facilities. Set $\mathcal{A}^3$ consists of arcs that directly connect suppliers to biorefineries; and set $\mathcal{A}^4$ consists of arcs connecting biorefineries to markets. Travel distance along arcs in $\mathcal{A}^1$ is short. Thus biomass is shipped along these arcs by trucks. Transportation quantities along arcs in $\mathcal{A}^2$ are large, and transportation distances are typically long. Thus, transportation modes such as rail and barge are used to move biomass between hubs. We denote the unit cost along arcs $(i, j) \in \mathcal{A}^1$ and $(j, k) \in \mathcal{A}^2$ by c_{ijkt}. These costs are equal to $c_{ijkt} = c_{ijt} + c_{jkt}$. Arcs in $\mathcal{A}^3$ represent direct shipments of biomass from suppliers to biofuel plants. These arcs are used to consider the scenario when a supplier is located nearby a biofuel plant, and therefore, direct truck shipments are delivered. Biomass, when delivered by rail or barge, is transported using cargo containers. Therefore, for rail and barge transportation, in addition to the variable unit transportation cost, this study considers that a fixed cost ξ_{jkt}, represents the costs associated with the loading and unloading of containers, occurs in period t. Container capacity is denoted by v^{cap}. Biofuel is transported by truck from biofuel plants to the market. We assume that all of the costing parameters, variable and fixed, will vary over the planning horizon.

In our model setting, the first hubs, the consolidation points, need storage capacities. We facilitate this via the use of capacity parameters, c_{lj}^{cap}. This is because, rail cars from different suppliers would be waiting at this consolidation point until a dedicated unit train is created consisting of 60–90 rail cars of biomass from different suppliers to be delivered to a single plant. Delivery of biomass via dedicated unit trains is a must to minimize biomass delivery costs. Otherwise, the cost of delivering biomass via small rail shipment consisting of a few rail cars is not economical. This assumption (about dedicated unit rail) is based on the outcomes of a recent report from the Idaho National Lab (INL), which describes structural elements of a biofuel supply chain that would meet our future needs for biofuels (Hess et al. 2009). Since each train has a unique destination, then the second hub (deconsolidation point) does not have much role in this supply chain. The unit train is delivered at the biorefinery, and biomass is stored there. This is another motivation why the second hub is merged with biorefineries. Now, at the biorefinery, we do consider capacities: production capacity (p_{lk}^{cap}) and storage capacity (h_{lk}^{cap}). The sets, input parameters, and decision variables used in this section are described in Table 1.

The following decision variables are introduced:

$$Y_{ljt} = \begin{cases} 1 & \text{if the multimodal facility } j \text{ of capacity } l \text{ is used in time period } t, \\ 0 & \text{otherwise;} \end{cases} \quad \forall\, l \in \mathcal{L}^h;\ j \in \mathcal{J};\ t \in \mathcal{T}.$$

$$Y_{lk} = \begin{cases} 1 & \text{if a biofuel plant of capacity } l \text{ is opened at location } k, \\ 0 & \text{otherwise;} \end{cases} \quad \forall\, l \in \mathcal{L}^b;\ k \in \mathcal{K}.$$

Variables Z_{jkt} identify the number of containers used between facilities j and k in period t. Variables P_{lkt} represent the amount of biofuel produced at biofuel

Table 1. Description of the Sets, Parameters, and Decision Variables

Symbol	Description
	Sets
$\mathcal{I}$	Set of harvesting sites (farms)
$\mathcal{J}$	Set of multimodal facilities (hubs)
$\mathcal{K}$	Set of potential locations for biofuel plants
$\mathcal{H}$	Set of multimodal facilities and biofuel plants; i.e., $\mathcal{H} = \mathcal{J} \cup \mathcal{K}$
$\mathcal{G}$	Set of markets
$\mathcal{L}^b$	Set of production capacities for biofuel plants
$\mathcal{L}^h$	Set of storage capacities for multimodal facilities
$\mathcal{T}$	Set of time periods
	Parameters
Ψ_{ljt}	Fixed cost of using a hub of capacity $l \in \mathcal{L}^h$ at location $j \in \mathcal{J}$ in time period $t \in \mathcal{T}$
η_{ljt}	Recovery gain associated with discontinued use of a hub of capacity l at j in period t
Ψ_{lk}	Fixed cost of opening a biofuel plant of capacity $l \in \mathcal{L}^b$ at location $k \in \mathcal{K}$
ξ_{jkt}	Fixed cost of a cargo container for transporting biomass along arc $(j,k) \in \mathcal{A}^2$ in period t
c_{lkt}	Unit flow cost along arc $(l,k) \in \mathcal{A}$ in period t
p_{lkt}	Unit production cost at a biofuel plant of size l located at k in period t
h_{kt}	Unit inventory cost at biofuel plant k in period t
π_{gt}	Unit penalty cost of not satisfying demand of market g in period t
s_{it}	Amount of biomass available at site $i \in \mathcal{I}$ in period t
b_{gt}	Biofuel demand of market $g \in \mathcal{G}$ in period t
c_{lj}^{cap}	Biomass storage/handling capacity of a multimodal facility of size $l \in \mathcal{L}^h$ at location j
h_{lk}^{cap}	Biomass storage capacity of a biofuel plant of size $l \in \mathcal{L}^b$ at location k
v^{cap}	Cargo container capacity
p_{lk}^{cap}	Production capacity of a biofuel plant of size l at location k
ϕ	Conversion rate from biomass to biofuel
q_{jt}	Failure probability of multimodal facility j in time period t
	Decision variables
Y_{lk}	If a biofuel plant of capacity l is opened at location k; 0 otherwise
Y_{ljt}	If the multimodal facility j of capacity l is used in time period t; 0 otherwise
Z_{jkt}	Number of containers used between facilities j and k in period t
X_{ijt}	Amount shipped along $(i,j) \in \mathcal{A}$ in period t
X_{ijkt}	Amount of biomass delivered in period t from supplier i to biofuel plant k though facilities j and k
X_{kgt}	Amount of biofuel delivered to demand city g from biofuel plant k in period t
P_{lkt}	Amount of biofuel produced at biofuel plant k of capacity l in period t
H_{kt}	Amount of biomass stored at biofuel plant k in period t
U_{gt}	Amount of unsatisfied demand in market g in period t

plant k of capacity l in period t. Variables H_{kt} represent the amount of biomass stored at biofuel plant k in period t, and U_{gt} represents the amount of unsatisfied demand in market g in period t.

We assume that each hub is disrupted independently. Although it may seem simplified, there is a reason behind this assumption. Consider the location of the main hubs of Delta Air Lines in the United States: Detroit, Atlanta, New York, Minneapolis, and Salt Lake City. These Delta hubs are located far away from one another. Similarly, since hubs are shipment consolidation points, the chances are they are located away from one another, and therefore will not be affected by the same disruptions. We denote by q_{jt} the disruption probability of hub $j \in \mathcal{J}$ in period t. Thus, $(1-q_{jt})$ is the probability that this hub is operating during time t. A shipment can be delivered to a biofuel plant through the multimodal transportation network if both the facilities j and k are operating. This happens with a probability of $(1-q_{jt})(1-q_{kt})$. The probability that either or both facilities fail is $(q_{jt}+q_{kt}-q_{jt}q_{kt})$. The coefficient βc_{ijkt} represents the unit emergency service costs to deliver the product in case of a disruption. One can think of β as a representation of the decision-maker's attitude toward risk. A risk averse decision maker would assign β a high value; and a risk pro decision maker assigns β small values. Since β depends on the decision-maker's attitude toward risk, and we assume a centralized system, the value of beta is independent of facility location. We assume that direct truck shipments are not affected by disruptions. Let X_{ijt} represent the amount shipped along $(i,j) \in \mathcal{A}$ in period t; and X_{ijkt} represent the amount of biomass delivered in period t from supplier i to biofuel plant k though facilities j and k. Then, the expected variable transportation cost along the multimodal transportation network is

$$\sum_{t\in\mathcal{T}}\Bigg[\sum_{i\in\mathcal{I},\,j\in\mathcal{J},\,k\in\mathcal{K}}\big(c_{ijkt}(1-q_{jt})(1-q_{kt})X_{ijkt} +\beta c_{ijkt}(q_{jt}+q_{kt}-q_{jt}q_{kt})X_{ijkt}\big)+\sum_{(i,j)\in\mathcal{A}^3}c_{ijt}X_{ijt}\Bigg].$$

The problem is to identify where to locate biorefineries among the candidate locations $k \in \mathcal{K}$; what should be the production capacity of each biofuel plant; which transportation hub to use or discontinue using in period t; and how much biomass to deliver to a biofuel plant, how much biomass to keep in the inventory, and how much biofuel to deliver to the markets in each time period. The goal is to minimize the total system costs under normal and hub disruption scenarios. The following is an MINLP formulation of the problem referred to as model [DR]:

$$\begin{aligned}
&\text{[DR]}\\
&\text{minimize}\sum_{l\in\mathcal{L}^b,\,k\in\mathcal{K}}\Psi_{lk}Y_{lk}\\
&+\sum_{t\in\mathcal{T}}\Bigg[\sum_{l\in\mathcal{L},\,j\in\mathcal{J}}\big(\Psi_{ljt}Y_{ljt}(1-Y_{lj,t-1})-\eta_{ljt}Y_{lj,t-1}(1-Y_{ljt})\big)\\
&\quad+\sum_{(j,k)\in\mathcal{A}^2}\xi_{jkt}Z_{jkt}+\sum_{i\in\mathcal{I},j\in\mathcal{J},k\in\mathcal{K}}c_{ijkt}\\
&\quad\cdot\big((1-q_{jt})(1-q_{kt})X_{ijkt}+\beta(q_{jt}+q_{kt}-q_{jt}q_{kt})X_{ijkt}\big)\\
&\quad+\sum_{(i,k)\in\mathcal{A}^3}c_{ikt}X_{ikt}+\sum_{(k,g)\in\mathcal{A}^4}c_{kgt}X_{kgt}\\
&\qquad+\sum_{l\in\mathcal{L}^b,\,k\in\mathcal{K}}p_{lkt}P_{lkt}+\sum_{k\in\mathcal{K}}h_{kt}H_{kt}+\sum_{g\in\mathcal{G}}\pi_{gt}U_{gt}\Bigg]
\end{aligned}$$

subject to

$$\sum_{k\in\mathcal{K}} X_{ikt} + \sum_{j\in\mathcal{J},k\in\mathcal{K}} X_{ijkt} \le s_{it} \quad \forall i\in\mathcal{I}, t\in\mathcal{T}, \tag{1}$$

$$\phi\left[\sum_{i\in\mathcal{I}} X_{ikt} + \sum_{(i,j)\in\mathcal{A}^1} X_{ijkt} + H_{k,t-1} - H_{kt}\right] = \sum_{l\in\mathcal{L}^b} P_{lkt}, \quad \forall k\in\mathcal{K}, t\in\mathcal{T}, \tag{2}$$

$$\sum_{g\in\mathcal{G}} X_{kgt} \le \sum_{l\in\mathcal{L}^b} P_{lkt}, \quad \forall k\in\mathcal{K}, t\in\mathcal{T}, \tag{3}$$

$$\sum_{k\in\mathcal{K}} X_{kgt} + U_{gt} = b_{gt}, \quad \forall g\in\mathcal{G}, t\in\mathcal{T}, \tag{4}$$

$$\sum_{i\in\mathcal{I},k\in\mathcal{K}} X_{ijkt} \le \sum_{l\in\mathcal{L}^h} c_{lj}^{\text{cap}} Y_{ljt}, \quad \forall j\in\mathcal{J}, t\in\mathcal{T}, \tag{5}$$

$$\sum_{i\in\mathcal{I}} X_{ijkt} \le v^{\text{cap}} Z_{jkt}, \quad \forall (j,k)\in\mathcal{A}^2, t\in\mathcal{T}, \tag{6}$$

$$P_{lkt} \le p_{lk}^{\text{cap}} Y_{lk}, \quad \forall l\in\mathcal{L}^b, k\in\mathcal{K}, t\in\mathcal{T}, \tag{7}$$

$$H_{kt} \le \sum_{l\in\mathcal{L}^b} h_{lk}^{\text{cap}} Y_{lk}, \quad \forall k\in\mathcal{K}, t\in\mathcal{T}, \tag{8}$$

$$\sum_{l\in\mathcal{L}^b} Y_{lk} \le 1, \quad \forall k\in\mathcal{K}, \tag{9}$$

$$Y_{lk}\in\{0,1\}, \quad \forall l\in\mathcal{L}^b, k\in\mathcal{K}, \tag{10}$$

$$Y_{ljt}\in\{0,1\}, \quad \forall l\in\mathcal{L}^h, j\in\mathcal{J}, t\in\mathcal{T}, \tag{11}$$

$$Z_{jkt}\in Z^+, \quad \forall j\in\mathcal{J}, k\in\mathcal{K}, t\in\mathcal{T}, \tag{12}$$

$$X_{ijkt}, X_{ikt}, X_{kgt}, P_{lkt}, H_{kt}, U_{gt} \ge 0, \quad \forall i\in\mathcal{I}, j\in\mathcal{J}, k\in\mathcal{K}, g\in\mathcal{G}, t\in\mathcal{T}. \tag{13}$$

The objective function minimizes the total expected system costs. More specifically, the first term represents the fixed plant location cost. The second and third terms represent the costs of using and discontinued use of hubs. The fourth term represents the fixed cost of transporting cargo containers between intermodal hubs. The fifth and sixth terms represent the expected transportation costs under normal and disruption conditions. The seventh term represents truck transportation costs for direct shipments of biomass. The eighth term represents biofuel transportation costs. The ninth and tenth terms represent the cost associated with producing biofuel and holding biomass in the inventory. The last term of the objective function represents the penalty cost for unsatisfied demand.

Constraints (1) indicate that the amount of biomass shipped from supplier i in period t is limited by biomass availability. Constraints (2) are the flow conservation constraints at biofuel plants. These constraints indicate that the amount of biofuel produced in period t is limited by the amount of biomass shipped in that period and the available inventories. If a biofuel plant only holds biomass inventories, capital investments for such plants will be extremely high. Therefore, to deal with biomass supply uncertainties, biomass inventory should be held to maximize utilization of the existing production capacity. Constraints (3) indicate that the amount of biofuel delivered to the market is limited by the amount of biofuel produced in period t. Constraints (4) indicate whether demand for biofuel will be fulfilled through the hub-and-spoke distribution network or through substitute products available in the market. Constraints (5) indicate that the total amount of biomass shipped through a multimodal facility is limited by its capacity. Constraints (6) show that the amount of biomass shipped between hubs is limited by the number of available containers and container capacity. Constraints (7) are the biofuel production capacity limitations at a plant. Constraints (8) are the biomass storage limitations at a biofuel plant. Constraints (9) ensure that, at most, one biofuel plant is operating at a particular location in period t. Constraints (10) and (11) are the binary constraints, and (12) are the integer constraints. Constraints (13) are the nonnegativity constraints.

3.2. A Linear Model Formulation

Model [DR] is nonlinear because of the $Y_{ljt}(1-Y_{lj,t-1})$ and $Y_{lj,t-1}(1-Y_{ljt})$ expressions in the objective function. The term $Y_{ljt}Y_{lj,t-1}$ in these expressions is the product of two binary decision variables, and therefore it takes values 0 and 1. We use the following technique to linearize model [DR] (Ghaderi, Boland, and JabalAmeli 2012).

Let F_{ljt} be a new binary variable that is equal to $Y_{lj,t-1}Y_{ljt}$. Let $\bar{R}_{ljt}$ and $\hat{R}_{ljt}$ be two decision variables defined as follows:

$$\bar{R}_{ljt} = Y_{ljt}(1-Y_{lj,t-1}) = Y_{ljt} - F_{ljt}, \quad \forall l\in\mathcal{L}^h, j\in\mathcal{J}, t\in\mathcal{T}, \tag{14}$$

$$\hat{R}_{ljt} = Y_{lj,t-1}(1-Y_{ljt}) = Y_{lj,t-1} - F_{ljt}, \quad \forall l\in\mathcal{L}^h, j\in\mathcal{J}, t\in\mathcal{T}. \tag{15}$$

By simplifying constraints (14) and (15) we obtain the following:

$$Y_{lj,t-1} + \bar{R}_{ljt} = Y_{ljt} + \hat{R}_{ljt}, \quad \forall l\in\mathcal{L}^h, j\in\mathcal{J}, t\in\mathcal{T}, \tag{16}$$

$$\bar{R}_{ljt}, \hat{R}_{ljt}\in\{0,1\}, \quad \forall l\in\mathcal{L}^h, j\in\mathcal{J}, t\in\mathcal{T}. \tag{17}$$

Since constraints (16) can be viewed as a network flow problem, for a given $j\in\mathcal{J}$ and $l\in\mathcal{L}$, the polytope $\{(Y_{ljt},\bar{R}_{ljt},\hat{R}_{ljt})\in[0,1]^{3|T|}\colon\ Y_{lj,t-1}+\bar{R}_{ljt} = Y_{ljt}+\hat{R}_{ljt}, \forall t\in\mathcal{T}\}$ will have the integrality property. Therefore, the resulting mechanism will provide a tight linear programming formulation for model [DR]. The new linear formulation of model [DR] is denoted by [LDR] and it is presented below

[LDR]

$$\begin{aligned}\text{minimize} \quad & \sum_{l\in\mathcal{L}^b,k\in\mathcal{K}} \Psi_{lk} Y_{lk} \\ & + \sum_{t\in\mathcal{T}}\Bigg[\sum_{l\in\mathcal{L}^h,j\in\mathcal{J}} (\Psi_{ljt}\bar{R}_{ljt} - \eta_{ljt}\hat{R}_{ljt}) + \sum_{(i,j)\in\mathcal{A}^2} \xi_{ijt} Z_{ijt} \\ & + \sum_{(i,k)\in\mathcal{A}^3} c_{ikt} X_{ikt} + \sum_{(k,g)\in\mathcal{A}^4} c_{kgt} X_{kgt} + \sum_{i\in\mathcal{I},j\in\mathcal{J},k\in\mathcal{K}} c_{ijkt}\end{aligned}$$

$$\cdot\big((1-q_{jt})(1-q_{kt})X_{ijkt}+\beta(q_{jt}+q_{kt}-q_{jt}q_{kt})X_{ijkt}\big)$$
$$+\sum_{l\in\mathcal{L}^b,k\in\mathcal{K}}p_{lkt}P_{lkt}+\sum_{k\in\mathcal{K}}h_{kt}H_{kt}+\sum_{g\in\mathcal{G}}\pi_{gt}U_{gt}\Big],$$

subject to (1)–(13) and (16)–(17).

To demonstrate the benefits of using the model proposed in this research, we compare its performance with the following three models: (a) minimum cost model, (b) reliable and static model, and (c) reliable and dynamic model. We refer to [LDR] as the reliable and dynamic model. The reliable and static model is a special case of [LDR], which considers that once a multimodal facility opens, it will continue to be available for use. Therefore, the fixed multimodal facility cost is paid from the period the facility is open, and thereafter. The minimum cost model does not consider disruptions; the model considers that hubs will be dynamically used throughout the year. This can be obtained by setting the value of $\{q_{jt}\}_{j\in\mathcal{J},t\in\mathcal{T}}=\{q_{kt}\}_{k\in\mathcal{K},t\in\mathcal{T}}=0.0$ in the objective function of [LDR].

4. Solution Approaches

Problem [LDR] is $\mathcal{NP}$-hard since a special case of this problem is the capacitated facility location problem. Therefore, commercial solvers, such as CPLEX, cannot solve large-scale instances of this problem. In this section we propose the following approaches to solve [LDR]: a rolling horizon heuristic, a greedy rolling horizon heuristic, a Benders decomposition algorithm, and a Benders-based rolling horizon algorithm. The goal is to generate a near optimal solution for [LDR] in a reasonable amount of time.

Benders decomposition separates the problem into a master problem and a subproblem. The master problem focuses on strategic decisions that are the facility location and capacity decisions; hub selection decisions; and transportation capacity decisions. The subproblem, which we solve for fixed values of some of the integer variables, is a linear program. The subproblem is an extension of the capacitated transportation problem, thus it is easy to solve. The master problem is a challenging problem to solve because it is an integer program. However, we efficiently solve the problem by adding valid inequalities, such as, the Pareto-optimal cuts, knapsack inequalities, logistics constraints, and integer cuts. Because of the structure of [LDR], if we were to decompose the problem in some other way, then we would be losing the structural properties in the subproblems. For example, if we were to use Lagrangian relaxation and relax constraints (2); then the problem would be decomposed by time period into $|\mathcal{T}|$ smaller-sized problems. Each subproblem would then be easier to solve. However, the corresponding subproblems lose information about the inventory holding and its relationships to the inflow and outflow in a facility. To overcome this drawback, we propose to solve the problem using a rolling horizon heuristic. This heuristic solves the problem iteratively $|\mathcal{T}|$ times. In iteration τ $(0\le\tau\le|\mathcal{T}|)$ a simpler problem is solved by fixing some of the integer variables. The hybrid Benders-based rolling horizon algorithm uses Benders algorithm to solve the subproblems created in each iteration of the rolling horizon algorithm. This algorithm takes advantage of our efficient Benders decomposition algorithm to solve the easier, time-restricted, subproblems solved during the RH algorithm. Both algorithms presented here complement one another. Whereas the accelerated Benders algorithm finds near optimal solutions for solving small to medium size network problems; the RH-Benders provides high-quality feasible solutions within a reasonable amount of time in solving large-size problem instances.

4.1. A Rolling Horizon Heuristic

This algorithm is based on the rolling horizon scheme proposed by Balasubramanian and Grossmann (2004) and Kostina et al. (2011). The approach is suitable for large-scale problems where solving the overall problem exactly is computationally intractable. Based on this approach, the original problem is decomposed into a series of smaller subproblems. Each subproblem comprises a few consecutive periods during the planning horizon. These subproblems—which are of a smaller size—are solved sequentially. Figure 3 shows how we use the rolling horizon approach to solve a problem with three time periods.

Let t_0^s denote the starting time period of subproblem s. Let N^s denote the number of time periods comprised in subproblem s. Depending on the type of problem solved, N^s could be different or could be the same for all of the subproblems created. The number of time periods within each subproblem stays fixed at N. We call *approximate subproblem* s the following approximation of problem [LDR]:

- Time horizon starts in period t_0^s and ends in period T.
- $Y_{ljt}\in\{0,1\}$ and $Z_{jkt}\in Z^+$ for $t_0^s\le t\le t_0^s+N$.
- $0\le Y_{ljt}\le 1$ and $Z_{jkt}\in R^+$ for $t>t_0^s+N$.
- The values of Y_{ljt} and Z_{jkt} for $t<t_0^s$ are fixed to the values found when solving approximate subproblem $s-1$.

Let [RH] denote the rolling horizon algorithm described below. Let [RH(s)] denote the sth approximate subproblem that is solved during the sth iteration of the algorithm.

***Step* 1.** Initialize; set starting time period to $t_0^s=0$; set the length of time interval to N; set $s\leftarrow 1$.

Figure 3. Application of a Rolling Horizon Strategy for a Three Time Period Problem

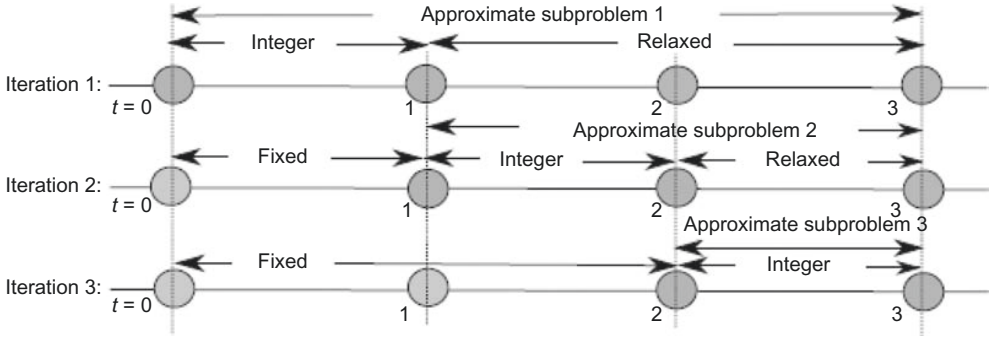

***Step* 2.** Solve the approximate subproblem [RH(s)] using CPLEX.

***Step* 3.** If $t_0 > |\mathcal{T}|$, then *Stop*; else, set $s \leftarrow s+1$, go to Step 2.

4.2. A Greedy Rolling Horizon Heuristic

The most time-consuming step of the [RH] algorithm is solving the first approximate subproblem [RH(1)], mainly because of its large size. Therefore, when solving [RH(1)] using CPLEX (Step 2 of [RH]), to optimize the running time of [RH], the algorithm stops as soon as a feasible solution is found. Once subproblem [RH(1)] is solved, the corresponding integer variables are fixed. Typically, the remaining subproblems are easier to solve.

To tackle this challenge with [RH], we adopt the following greedy approach, denoted by **[GRH]**. This approach solves the original problem [LDR] for $t = 1$ only. Next, the values of Y_{lj1} and Z_{jk1} are fixed, and the problem for the remaining time periods is solved by using [RH]. The steps of **[GRH]** are described below:

***Step* 1.** Solve problem [LDR] for $t = 1$.

***Step* 2.** Fix the Y_{lj1} and Z_{jk1} variables obtained from Step 1, and apply [RH] algorithm to solve the problem for the remaining time periods.

4.3. Benders Decomposition

The algorithm described in this section is an extension of the Benders decomposition method proposed by Benders (1962). Benders decomposition is a well-known partitioning method used to solve mixed-integer linear programs. The motivation for selecting this method is the structure of formulation [LDR]. The algorithm separates the original problem into two subproblems: an integer *master problem* and a linear *subproblem*. The underlying Benders reformulation for [LDR] is the following:

$$\begin{aligned}\text{minimize}\quad & \sum_{l\in\mathcal{L}^b,k\in\mathcal{K}} \Psi_{lk} Y_{lk} \\ & + \sum_{t\in\mathcal{T}}\left\{\sum_{l\in\mathcal{L}^h,j\in\mathcal{J}} (\Psi_{ljt}\bar{R}_{ljt} - \eta_{ljt}\hat{R}_{ljt}) + \sum_{(i,j)\in\mathcal{A}^2} \xi_{ijt} Z_{ijt}\right\}. \\ & + [\text{LDR-SUB}](X,U,P,H \mid \hat{Y}^b, \hat{Y}^h, \hat{Z}) \\ \text{subject to}\quad & (1)\text{–}(13) \text{ and } (16)\text{–}(17).\end{aligned}$$

$[\text{LDR-SUB}](X,U,P,H \mid \hat{Y}^b, \hat{Y}^h, \hat{Z})$ represents the Benders subproblem, which is presented below. In this subproblem, the values of $Y^b := \{Y_{lk} \mid l \in \mathcal{L}^b, k \in \mathcal{K}\}$, $Y^h := \{Y_{ljt} \mid l \in \mathcal{L}^h, j \in \mathcal{J}, t \in \mathcal{T}\}$, and $Z := \{Z_{jkt} \mid j \in \mathcal{J}, k \in \mathcal{K}, t \in \mathcal{T}\}$ are given and satisfy constraints (10)–(13) and (16)–(17). Therefore, this subproblem has only continuous variables

[LDR-SUB]

$$\begin{aligned}\text{minimize}\quad & \sum_{t\in\mathcal{T}}\Bigg\{\sum_{i\in\mathcal{I},j\in\mathcal{J},k\in\mathcal{K}} c_{ijkt}((1-q_{jt})(1-q_{kt})X_{ijkt} \\ & + \beta(q_{jt}+q_{kt}-q_{jt}q_{kt})X_{ijkt}) \\ & + \sum_{(i,k)\in\mathcal{A}^3} c_{ikt}X_{ikt} + \sum_{(k,g)\in\mathcal{A}^4} c_{kgt}X_{kgt} \\ & + \sum_{l\in\mathcal{L}^b,k\in\mathcal{K}} p_{lkt}P_{lkt} + \sum_{k\in\mathcal{K}} h_{kt}H_{kt} + \sum_{g\in\mathcal{G}} \pi_{gt}U_{gt}\Bigg\}\end{aligned}$$

subject to

$$\sum_{k\in\mathcal{K}} X_{ikt} + \sum_{j\in\mathcal{J},k\in\mathcal{K}} X_{ijkt} \le s_{it}(\delta_{it}), \quad \forall\, i\in\mathcal{I},\ t\in\mathcal{T}, \tag{18}$$

$$\phi\left[\sum_{i\in\mathcal{I}} X_{ikt} + \sum_{(i,j)\in\mathcal{A}^1} X_{ijkt} + H_{k,t-1} - H_{kt}\right] = \sum_{l\in\mathcal{L}^b} P_{lkt}(\vartheta_{kt}), \quad \forall\, k\in\mathcal{K},\ t\in\mathcal{T}, \tag{19}$$

$$\sum_{g\in\mathcal{G}} X_{kgt} \le \sum_{l\in\mathcal{L}} P_{lkt}(\Phi_{kt}), \quad \forall\, k\in\mathcal{K},\ t\in\mathcal{T}, \tag{20}$$

$$\sum_{k\in\mathcal{K}} X_{kgt} + U_{gt} = b_{gt}(\gamma_{gt}), \quad \forall\, g\in\mathcal{G},\ t\in\mathcal{T}, \tag{21}$$

$$\sum_{i\in\mathcal{I},k\in\mathcal{K}} X_{ijkt} \le \sum_{l\in\mathcal{L}^h} c^{\text{cap}}_{lj}\hat{Y}_{ljt}(\chi_{jt}), \quad \forall\, j\in\mathcal{J},\ t\in\mathcal{T}, \tag{22}$$

$$\sum_{i\in\mathcal{I}} X_{ijkt} \le v^{\text{cap}}\hat{Z}_{jkt}(\mu_{jkt}), \quad \forall\,(j,k)\in\mathcal{A}^2,\ t\in\mathcal{T}, \tag{23}$$

$$P_{lkt} \le p^{\text{cap}}_{lk}\hat{Y}_{lk}(\kappa_{lkt}), \quad \forall\, l\in\mathcal{L}^b,\ k\in\mathcal{K},\ t\in\mathcal{T}, \tag{24}$$

$$H_{kt} \le \sum_{l\in\mathcal{L}^b} h^{\text{cap}}_{lk}\hat{Y}_{lk}(\varsigma_{kt}), \quad \forall\, k\in\mathcal{K},\ t\in\mathcal{T}, \tag{25}$$

$$X_{ijkt}, X_{ikt}, X_{kgt}, P_{lkt}, H_{kt}, U_{gt} \ge 0, \quad \forall\, i\in\mathcal{I},\ j\in\mathcal{J},\ k\in\mathcal{K},\ g\in\mathcal{G},\ t\in\mathcal{T}. \tag{26}$$

Note that, because of the presence of variables U_{gt} in constraints (21), formulation [LDR] will always generate a feasible solution that satisfies demand. This

is because the model formulation allows substitute products—which are assumed to be available in the market—to satisfy demand if the supply chain cannot.

Let $\delta = \{\delta_{it} \geq 0 \,|\, i \in \mathcal{I}, t \in \mathcal{T}\}$, $\vartheta = \{\vartheta_{kt} \,|\, k \in \mathcal{K}, t \in \mathcal{T}\}$, $\Phi = \{\Phi_{kt} \geq 0 \,|\, k \in \mathcal{K}, t \in \mathcal{T}\}$, $\gamma = \{\gamma_{gt} \,|\, g \in \mathcal{G}, t \in \mathcal{T}\}$, $\chi = \{\chi_{jt} \geq 0 \,|\, j \in \mathcal{J}, t \in \mathcal{T}\}$, $\mu = \{\mu_{jkt} \geq 0 \,|\, j \in \mathcal{J}, k \in \mathcal{K}, t \in \mathcal{T}\}$, $\kappa = \{\kappa_{lkt} \geq 0 \,|\, l \in \mathcal{L}, k \in \mathcal{K}, t \in \mathcal{T}\}$, and $\varsigma = \{\varsigma_{kt} \geq 0 \,|\, k \in \mathcal{K}, t \in \mathcal{T}\}$ be the dual variables associated with constraints (18)–(25), respectively. The dual of the primal subproblem, called the *dual subproblem* [LDR-SUB(D)], can be written as

[LDR-SUB(D)]

$$\begin{aligned}\text{maximize} \quad & \sum_{t\in\mathcal{T}}\Bigg\{\sum_{g\in\mathcal{G}} b_{gt}\gamma_{gt} - \sum_{i\in\mathcal{I}} s_{it}\delta_{it} - \sum_{l\in\mathcal{L}^h, j\in\mathcal{J}} c^{\text{cap}}_{lj}\hat{Y}_{ljt}\chi_{jt} \\ & - \sum_{(i,j)\in\mathcal{A}^2} v^{\text{cap}}\hat{Z}_{ijt}\mu_{ijt} - \sum_{l\in\mathcal{L}^b, k\in\mathcal{K}} p^{\text{cap}}_{lk}\hat{Y}_{lk}\kappa_{lkt} \\ & - \sum_{l\in\mathcal{L}^b, k\in\mathcal{K}} h^{\text{cap}}_{lk}\hat{Y}_{lk}\varsigma_{kt}\Bigg\}\end{aligned}$$

subject to

$$\begin{aligned}& -\delta_{it} - \chi_{jt} - \mu_{jkt} + \phi\vartheta_{kt} \\ & \quad \leq c_{ijkt}\big((1-q_{jt})(1-q_{kt}) + \beta(q_{jt}+q_{kt}-q_{jt}q_{kt})\big), \\ & \qquad \forall i\in\mathcal{I}, j\in\mathcal{J}, k\in\mathcal{K}, t\in\mathcal{T}, \quad (27)\\ & -\delta_{it} + \phi\vartheta_{kt} \leq c_{ikt}, \quad \forall (i,k)\in\mathcal{A}^3, t\in\mathcal{T}, \quad (28)\\ & \gamma_{gt} - \Phi_{kt} \leq c_{kgt}, \quad \forall (k,g)\in\mathcal{A}^4, t\in\mathcal{T}, \quad (29)\\ & -\vartheta_{kt} + \Phi_{kt} - \kappa_{lkt} \leq p_{lkt}, \\ & \qquad \forall l\in\mathcal{L}^h, k\in\mathcal{K}, t\in\mathcal{T}, \quad (30)\\ & \phi\vartheta_{k,t+1} - \phi\vartheta_{kt} - \varsigma_{kt} \leq h_{kt}, \quad \forall k\in\mathcal{K}, t\in\mathcal{T}, \quad (31)\\ & \gamma_{gt} \leq \pi_{gt}, \quad \forall g\in\mathcal{G}, t\in\mathcal{T}, \quad (32)\\ & \delta,\chi,\mu,\Phi,\kappa,\varsigma\in\mathbb{R}^+, \quad (33)\\ & \gamma,\vartheta\in\mathbb{R}. \quad (34)\end{aligned}$$

Let θ represent the objective function value of the subproblem. Then, Benders *master problem* is represented as follows [LDR-M]:

[LDR-M]

$$\begin{aligned}\text{minimize} \quad & \sum_{l\in\mathcal{L}^b, k\in\mathcal{K}} \Psi_{lk}Y_{lk} \\ & + \sum_{t\in\mathcal{T}}\Bigg\{\sum_{l\in\mathcal{L}^h, j\in\mathcal{J}} (\Psi_{ljt}\bar{R}_{ljt} - \eta_{ljt}\hat{R}_{ljt}) + \sum_{(i,j)\in\mathcal{A}^2}\xi_{ijt}Z_{ijt}\Bigg\} + \theta\end{aligned}$$

subject to

$$\begin{aligned}& \theta + \sum_{t\in\mathcal{T}}\Bigg\{\sum_{i\in\mathcal{I}} s_{it}\delta_{it} + \sum_{l\in\mathcal{L}^h, j\in\mathcal{J}} c^{\text{cap}}_{lj}\chi_{jt}Y_{ljt}\Bigg\} \\ & \quad \geq \sum_{t\in\mathcal{T}}\Bigg\{\sum_{g\in\mathcal{G}} b_{gt}\gamma_{gt} - \sum_{(i,j)\in\mathcal{A}^2} v^{\text{cap}}\mu_{ijt}Z_{ijt} \\ & \qquad - \sum_{l\in\mathcal{L}^b, k\in\mathcal{K}} p^{\text{cap}}_{lk}\kappa_{lkt}Y_{lk} - \sum_{l\in\mathcal{L}^b, k\in\mathcal{K}} h^{\text{cap}}_{lk}\varsigma_{kt}Y_{lk}\Bigg\}, \\ & \qquad \forall(\gamma,\delta,\chi,\mu,\kappa,\varsigma)\in\mathcal{P}_D, \quad (35)\end{aligned}$$

$$\begin{aligned}& Y_{lj,t-1} + \bar{R}_{ljt} = Y_{ljt} + \hat{R}_{ljt}, \quad \forall l\in\mathcal{L}^h, j\in\mathcal{J}, t\in\mathcal{T}, \quad (36)\\ & \sum_{l\in\mathcal{L}^b} Y_{lk} \leq 1, \quad \forall k\in\mathcal{K}, \quad (37)\\ & Y_{lk}\in\{0,1\}, \quad \forall l\in\mathcal{L}^b, k\in\mathcal{K}, \quad (38)\\ & Y_{ljt}\in\{0,1\}, \quad \forall l\in\mathcal{L}^h, j\in\mathcal{J}, t\in\mathcal{T}, \quad (39)\\ & \bar{R}_{ljt}, \hat{R}_{ljt}\in\{0,1\}, \quad \forall l\in\mathcal{L}^h, j\in\mathcal{J}, t\in\mathcal{T}, \quad (40)\\ & Z_{jkt}\in Z^+, \quad \forall j\in\mathcal{J}, k\in\mathcal{K}, t\in\mathcal{T}. \quad (41)\end{aligned}$$

In this formulation, constraints (35) are the *optimality cut* constraints, and $\mathcal{P}_D$ is the set of the extreme points of the feasible region of [LDR-SUB(D)]. Since θ is the optimal objective function value of [LDR-SUB], its value is an upper bound to the objective function value of the solution from [LDR-SUB(D)] for fixed values of $\hat{Y}^b$, $\hat{Y}^h$, $\hat{Z}$. Therefore,

$$\begin{aligned}\theta \geq \sum_{t\in\mathcal{T}}\Bigg\{\sum_{g\in\mathcal{G}} b_{gt}\gamma_{gt} - \sum_{i\in\mathcal{I}} s_{it}\delta_{it} - \sum_{l\in\mathcal{L}^h, j\in\mathcal{J}} c^{\text{cap}}_{lj}\chi_{jt}Y_{ljt} \\ - \sum_{(i,j)\in\mathcal{A}^2} v^{\text{cap}}\mu_{ijt}Z_{ijt} - \sum_{l\in\mathcal{L}^b, k\in\mathcal{K}} p^{\text{cap}}_{lk}\kappa_{lkt}Y_{lk} \\ - \sum_{l\in\mathcal{L}^b, k\in\mathcal{K}} h^{\text{cap}}_{lk}\varsigma_{kt}Y_{lkt}\Bigg\} \\ \forall(\gamma,\delta,\chi,\mu,\kappa,\varsigma)\in\mathcal{P}_D. \quad (42)\end{aligned}$$

To accelerate the running time of the master problem, we add the following inequalities:

$$Z_{jkt} \leq \sum_{l\in\mathcal{L}^h}\left\lceil\frac{c^{\text{cap}}_{lj}}{v^{\text{cap}}}\right\rceil Y_{ljt}, \quad \forall (j,k)\in\mathcal{A}^2, t\in\mathcal{T}, \quad (43)$$

$$Z_{jkt} \leq \sum_{l\in\mathcal{L}^b}\left\lceil\frac{c^{\text{cap}}_{lk}}{v^{\text{cap}}}\right\rceil Y_{lk}, \quad \forall (j,k)\in\mathcal{A}^2, t\in\mathcal{T}. \quad (44)$$

Inequalities (43) and (44) are valid for [LDR-M] since they present the relationship that exists between the binary facility location variables and the integer, container flow variables. The ratio $\lceil c^{\text{cap}}_{lj}/v^{\text{cap}}\rceil$ represents the maximum number of containers initiated from hub j to deliver the available biomass. This amount is an upper bound on the total biomass delivered to biofuel plant k. The ratio $\lceil c^{\text{cap}}_{lk}/v^{\text{cap}}\rceil$ represents the maximum number of containers to be received at biofuel plant k to fully utilize its capacity. That number is clearly an upper bound on the total number of containers received from hub j. Additionally, these inequalities set the number of containers to zero if no facility is located in some of the potential facility location sites. Computational experiments indicate that these valid inequalities significantly reduce the number of iterations of the Benders algorithm.

The master problem [LDR-M] provides an equivalent formulation of the original problem [LDR]. The challenge faced when solving [LDR-M] is the problem size. Note that the number of inequalities (35) is equal to the number of extreme points of the feasible region

of problem [LDR-SUB(D)]. This number could be very large. For this reason, we solve instead a *restricted master problem* [LDR-RM] that uses instead only a subset of $\mathcal{P}_D$ denoted by $\mathcal{P}_D^n \subset \mathcal{P}_D$. Therefore, problem [LDR-RM] is a relaxation of [LDR], and the optimal solution to the restricted problem provides a lower bound for [LDR].

The general idea of the standard Benders decomposition algorithm is to iteratively solve [LDR-RM]. In iteration n, subproblem [LDR-SUB(D)] is solved, and a new extreme point $p \in \mathcal{P}_D$ is identified and added to $\mathcal{P}_D^n = \mathcal{P}_D^{n-1} \cup p$. Next, the restricted master problem is solved. This procedure continues until the gap between the lower bound generated by solving the restricted master problem and the upper bound generated by solving the subproblem is smaller than some predetermined value ϵ.

Let UB^n and LB^n denote the upper and lower bound of [LDR] at iteration n. Let $\mathcal{P}_D^n$ denote the set of extreme points of [LDR-SUB(D)] at iteration n. The algorithm starts by solving [LDR-RM], which provides a lower bound for this problem. We fix the values of the corresponding integer and binary variables to $\hat{Y}_{lk}^n$ for $l \in \mathcal{L}^b, k \in \mathcal{K}$, $\hat{Y}_{ljt}^n$ for $l \in \mathcal{L}^h, j \in \mathcal{J}, t \in \mathcal{T}$, and $\hat{Z}_{jkt}^n$ for $(j,k) \in \mathcal{A}_2, t \in \mathcal{T}$. We use these values to solve the dual subproblem [LDR-SUB(D)]. A pseudocode of the basic Benders decomposition algorithm is provided below.

Let

$$z_{\text{MAS}}^n = \sum_{l \in \mathcal{L}^b, k \in \mathcal{K}} \Psi_{lk} Y_{lk}^n + \sum_{t \in \mathcal{T}} \left\{ \sum_{l \in \mathcal{L}_h, j \in \mathcal{J}} (\Psi_{ljt} \bar{R}_{ljt}^n - \eta_{ljt} \hat{R}_{ljt}^n) + \sum_{(i,j) \in \mathcal{A}^2} \xi_{ijt} Z_{ijt}^n \right\};$$

let z_{MP}^n denote the solution to [LDR-RM] and z_{SUB}^n denote the solution to [LDR-SUB(D)] during the nth iteration of the Benders decomposition algorithm.

Algorithm 1 (Benders decomposition)

$\text{UB}^n \leftarrow +\infty$, $\text{LB}^n \leftarrow -\infty$, $n \leftarrow 1$, ϵ, $\mathcal{P}_D \leftarrow 0$
terminate $\leftarrow$ **false**
while (*terminate* = **false**) **do**
  Solve [LDR-RM] to obtain $\{Y_{lk}^n\}_{l \in \mathcal{L}^b, k \in \mathcal{K}}$, $\{Y_{ljt}^n\}_{l \in \mathcal{L}^h, j \in \mathcal{J}, t \in \mathcal{T}}$, $\{Z_{ijt}^n\}_{(i,j) \in \mathcal{A}^2, t \in \mathcal{T}}$, z_{MP}^n, z_{MAS}^n
  if $(z_{\text{MP}}^n > \text{LB}^n)$ **then**
    $\text{LB}^n \leftarrow z_{\text{MP}}^n$
  end if
  Set:
    $\hat{Y}_{lk}^n = Y_{lk}^n$ for $l \in \mathcal{L}^b, k \in \mathcal{K}$
    $\hat{Y}_{ljt}^n = Y_{ljt}^n$ for $l \in \mathcal{L}^h, j \in \mathcal{J}, t \in \mathcal{T}$
    $\hat{Z}_{jkt}^n = Z_{jkt}^n$ for $(j,k) \in \mathcal{A}^2, t \in \mathcal{T}$
  Solve [LDR-SUB(D)] to obtain $(\gamma_{gt}, \delta_{it}, \chi_{gt}, \mu_{jkt}, \kappa_{lkt}, \varsigma_{kt}) \in \mathcal{P}_D$ and z_{SUB}^n
  if $(z_{\text{SUB}}^n + z_{\text{MAS}}^n < \text{UB}^n)$ **then**
    $\text{UB}^n \leftarrow z_{\text{SUB}}^n + z_{\text{MAS}}^n$
  end if
  if $((\text{UB}^n - \text{LB}^n)/\text{UB}^n \le \epsilon)$ **then**
    terminate $\leftarrow$ **true**
  else
    $\mathcal{P}_D^{n+1} = \mathcal{P}_D^n \cup \{(\gamma_{gt}, \delta_{it}, \chi_{gt}, \mu_{jkt}, \kappa_{lkt}, \varsigma_{kt})\}$
  end if
  $n \leftarrow n+1$
end while.

4.4. Enhancements of Benders Decomposition Algorithm

In this section we present a few different cuts that we have identified and used to improve the performance of Benders decomposition algorithm.

4.4.1. Pareto-Optimal Cuts. Magnanti and Wong (1981) introduce the *Pareto-optimal cuts*, which are added to the master problem. The motivation is to identify from a set of potential cuts which cut has the greatest impact on the quality of the master problem. Work by Roy (1986) and Wentges (1996) shows that Pareto-optimal cuts contribute to improving the performance of Benders algorithm by strengthening the cut added to the master problem in each iteration of the algorithm.

With respect to our problem, recall that an optimality cut (35) for [LDR-RM] is generated using the information from an optimal solution to [LDR-SUB(D)]. Subproblem [LDR-SUB(D)] is a transportation problem, which are known to have multiple optimal solutions (Uster and Agrahari 2011). This inherent degeneracy property of transportation problems implies that multiple optimality cuts can be generated in an iteration of Benders algorithm, therefore, identifying the single cut that greatly impacts the quality of the solution to [LDR-RM] is critical. This study adopts an approach proposed by Papadakos (2008) for implementing subproblem independent Pareto-optimal cuts. Papadakos (2008) shows that when the solution of the auxiliary problem depends on the solution to the dual Benders subproblem, then generating a Pareto-optimal cut is computationally challenging. This challenge is greater especially when the Benders subproblem is a difficult problem to solve. To remedy this problem, Papadakos (2008) proposes the *Modified Magnanti-Wong* (*MMW*) method that generates a Pareto-optimal cut using the concept of core points. A core point is located in the relative interior of the convex hull of feasible region and serves as a proxy for the optimal solution.

The following is the formulation of the *Modified Magnanti-Wong* (*MMW*) subproblem solved in each iteration of Benders algorithm instead of [LDR-SUB(D)]. We refer to this subproblem as [LDR-SUB(MMW)]. Let $\mathbb{Y}^{\text{LP}}$ be the polyhedron defined by (36), (37), $0 \le Y_{ljt} \le 1$, $\forall l \in \mathcal{L}$, $j \in \mathcal{J}$, $t \in \mathcal{T}$; $0 \le Y_{lk} \le 1$, $\forall l \in \mathcal{L}$, $k \in \mathcal{K}$; and $Z_{jkt} \ge 0$, $\forall j \in \mathcal{J}$, $k \in \mathcal{K}$, $t \in \mathcal{T}$. Let $\text{ri}(\mathbb{Y}^{\text{LP}})$ denote the relative interior of $\mathbb{Y}^{\text{LP}}$. A Pareto-optimal cut can

be obtained by solving the following subproblem, for $Y^0_{ljt} \in \text{ri}(\mathbb{Y}^{\text{LP}})$, $\forall l \in \mathcal{L}^h$, $j \in \mathcal{J}$, $t \in \mathcal{T}$; and $Y^0_{lk} \in \text{ri}(\mathbb{Y}^{\text{LP}})$, $\forall l \in \mathcal{L}^b$, $k \in \mathcal{K}$:

[LDR-SUB(MMW)]

$$\begin{aligned}\text{maximize} \sum_{t\in\mathcal{T}}\Bigg\{&\sum_{g\in\mathcal{G}} b_{gt}\gamma_{gt} - \sum_{i\in\mathcal{I}} s_{it}\delta_{it} - \sum_{l\in\mathcal{L},j\in\mathcal{J}} c^{\text{cap}}_{lj} Y^0_{ljt}\chi_{jt} \\ &- \sum_{(i,j)\in\mathcal{A}_2} v^{\text{cap}} Z^0_{ijt}\mu_{ijt} - \sum_{l\in\mathcal{L},k\in\mathcal{K}} p^{\text{cap}}_{lk} Y^0_{lk}\kappa_{lkt} \\ &- \sum_{l\in\mathcal{K},k\in\mathcal{K}} h^{\text{cap}}_{lk} Y^0_{lk}\varsigma_{kt}\Bigg\}\end{aligned}$$

subject to

$$\begin{aligned}&-\delta_{it} - \chi_{jt} - \mu_{jkt} + \phi\vartheta_{kt} \\ &\quad \le c_{ijkt}\big((1-q_{jt})(1-q_{kt}) + \beta(q_{jt}+q_{kt}-q_{jt}q_{kt})\big), \\ &\qquad \forall i\in\mathcal{I}, j\in\mathcal{J}, k\in\mathcal{K}, t\in\mathcal{T}, && (45)\\ &-\delta_{it} + \phi\vartheta_{kt} \le c_{ikt}, \quad \forall (i,k)\in\mathcal{A}^3, t\in\mathcal{T}, && (46)\\ &\gamma_{gt} - \Phi_{kt} \le c_{kgt}, \quad \forall (k,g)\in\mathcal{A}^4, t\in\mathcal{T}, && (47)\\ &-\vartheta_{kt} + \Phi_{kt} - \kappa_{lkt} \le p_{lkt}, \quad \forall l\in\mathcal{L}^h, k\in\mathcal{K}, t\in\mathcal{T}, && (48)\\ &\phi\vartheta_{k,t+1} - \phi\vartheta_{kt} - \varsigma_{kt} \le h_{kt}, \quad \forall k\in\mathcal{K}, t\in\mathcal{T}, && (49)\\ &\gamma_{gt} \le \pi_{gt}, \quad \forall g\in\mathcal{G}, t\in\mathcal{T}, && (50)\\ &\delta,\chi,\mu,\Phi,\kappa,\varsigma\in\mathbb{R}^+, && (51)\\ &\gamma,\vartheta\in\mathbb{R}. && (52)\end{aligned}$$

In this formulation, Y^0_{ljt}, Y^0_{lk}, and Z^0_{jkt} are core points. These points are updated as follows:

$$\begin{aligned}Y^0_{ljt} &= \tau Y^0_{ljt} + (1-\tau)\bar{Y}_{ljt}, \quad \forall l\in\mathcal{L}^h, j\in\mathcal{J}, t\in\mathcal{T},\\ Y^0_{lk} &= \tau Y^0_{lk} + (1-\tau)\bar{Y}_{lk}, \quad \forall l\in\mathcal{L}^b, k\in\mathcal{K},\\ Z^0_{jkt} &= \tau Z^0_{jkt} + (1-\tau)\bar{Z}_{jkt}, \quad \forall j\in\mathcal{J}, k\in\mathcal{K}, t\in\mathcal{T},\end{aligned}$$

where $\bar{Y}_{ljt}$, $\bar{Y}_{lk}$, and $\bar{Z}_{jkt}$ are the solutions obtained from the current master problem. Experimental results indicate that setting $\tau = 0.5$ provides the best empirical results. Note that the auxiliary subproblem [LDR-SUB(MMW)] is independent of the solutions obtained from the original dual subproblem ([LDR-SUB(D)]) and will assist the Benders master problem to be one step closer to the optimal solution from the very first iteration (Papadakos 2008).

4.4.2. Knapsack Inequalities. Santoso et al. (2005) show that when a good upper bound is available from the Benders decomposition algorithm, then adding a knapsack inequality—presented below—along with the optimality cut constraint (35) will improve the quality of solutions derived from the Benders master problem. The authors also point out that state-of-the-art solvers such as CPLEX can derive a variety of valid inequalities from the knapsack inequality, which expedites the convergence of the Benders decomposition algorithm. Let UB^n be the best-known upper bound obtained so far. The following valid inequality is added to the master problem [LDR-RM] in iteration $n+1$:

$$\begin{aligned}\text{UB}^n \ge \sum_{t\in\mathcal{T}}\Bigg\{&\sum_{l\in\mathcal{L}^h, j\in\mathcal{J}} (\Psi_{ljt}\bar{R}_{ljt} - \eta_{ljt}\hat{R}_{ljt}) \\ &+ \sum_{l\in\mathcal{L}^b,k\in\mathcal{K}} (\Psi_{lkt} - p^{\text{cap}}_{lk}\kappa_{lkt} - h^{\text{cap}}_{lk}\varsigma_{kt})Y_{lk} \\ &+ \sum_{(i,j)\in\mathcal{A}_2} (\xi_{ijt} - v^{\text{cap}}\mu_{ijt})Z_{ijt} + \sum_{g\in\mathcal{G}} b_{gt}\gamma_{gt} \\ &- \sum_{i\in\mathcal{I}} s_{it}\delta_{it} - \sum_{l\in\mathcal{L},j\in\mathcal{J}} c^{\text{cap}}_{lj} Y_{ljt}\chi_{jt}\Bigg\}. \qquad (53)\end{aligned}$$

Similarly, we add the following valid inequalities to the master problem [LDR-RM] to speed up the branch-and-bound procedure of the solver. Let LB^n denote the best-known lower bound obtained so far

$$\begin{aligned}\text{LB}^n \le &\sum_{l\in\mathcal{L}^b,k\in\mathcal{K}} \Psi_{lk}Y_{lk} \\ &+ \sum_{t\in\mathcal{T}}\Bigg\{\sum_{l\in\mathcal{L}^h,j\in\mathcal{J}} (\Psi_{ljt}\bar{R}_{ljt} - \eta_{ljt}\hat{R}_{ljt}) + \sum_{(i,j)\in\mathcal{A}_2}\xi_{ijt}Z_{ijt}\Bigg\} + \theta. \qquad (54)\end{aligned}$$

4.4.3. Logistics Constraints. In the initial stages of the Benders decomposition algorithm, the master problem produces very few first-stage decision variables. This is the case until sufficient information is gathered from solving the subproblem. To overcome this issue with the master problem, we add the following logistics constraints. The rationale is to bring to the master problem some information from the subproblem. Doing this will improve the running time of the Benders decomposition algorithm.

Recall the demand satisfying constraints described in Equation (4). Since this is a minimization problem, these constraints can be expressed as follows:

$$\sum_{k\in\mathcal{K}} X_{kgt} + U_{gt} \ge b_{gt}, \quad \forall g\in\mathcal{G}, t\in\mathcal{T}. \qquad (55)$$

Furthermore, constraints (3) and (7) can be rewritten as follows:

$$\sum_{g\in\mathcal{G}} X_{kgt} \le \sum_{l\in\mathcal{L}^b} p^{\text{cap}}_{lk} Y_{lk}, \quad \forall k\in\mathcal{K}, t\in\mathcal{T}. \qquad (56)$$

Combining constraints (55) and (56) and dropping the penalty term U_{gt} obtains the following inequalities that are added to the master problem:

$$\sum_{l\in\mathcal{L}^b,k\in\mathcal{K}} p^{\text{cap}}_{lk} Y_{lk} \ge \sum_{g\in\mathcal{G}} \bar{b}_{gt}, \quad \forall t\in\mathcal{T}. \qquad (57)$$

Here $\bar{b}_{gt}$ represents the amount of biofuel demand expected to be met through the supply chain network. Thus, $\bar{b}_{gt} = \alpha \times b_{gt}, \forall g\in\mathcal{G}, t\in\mathcal{T}$. We can initialize the value of α between 0.0 to 1.0; and when $\alpha = 1.0$, constraints (57) require that all of the demand is satisfied by this supply chain.

4.4.4. Integer Cuts. To expedite the running time of the master problem we add the following inequalities generated using a local branching technique (Fischetti and Lodi 2003). These inequalities when added to the master problem during iteration $n+1$, force the problem to generate a solution different from the solution generated during iteration n. In other words, adding these cuts to the master problem excludes from the feasible region the solutions identified in the previous iteration. Let $\hat{Y}^n_{ljt}$ for $l\in\mathcal{L}^h$, $j\in\mathcal{J}$, $t\in\mathcal{T}$ and $\hat{Y}^n_{lk}$ for $l\in\mathcal{L}^b$, $k\in\mathcal{K}$ be the solutions obtained from solving the master problem in iteration n. Let $\mathcal{Y}^n_1=\{(l,j,t)\,|\,\hat{Y}^n_{ljt}=1,\ \forall l\in\mathcal{L}^h,\ j\in\mathcal{J},\ t\in\mathcal{T}\}$ and $\mathcal{Y}^n_2=\{(l,k)\,|\,\hat{Y}^n_{lk}=1,\ \forall l\in\mathcal{L}^b,\ k\in\mathcal{K}\}$. We add the following constraint to the master problem in iteration $n+1$:

$$\sum_{(l,j,t)\in\mathcal{Y}^n_1}(1-Y_{ljt})+\sum_{(l,k)\in\mathcal{Y}^n_2}(1-Y_{lk})+\sum_{(l,j,t)\notin\mathcal{Y}^n_1}Y_{ljt}+\sum_{(l,k)\notin\mathcal{Y}^n_2}Y_{lk}\geq 1. \tag{58}$$

This inequality forces the values of the binary facility location variables in iteration $n+1$ to be different from iteration n. The two consecutive solutions will differ by at least one variable.

Similarly, to reduce the search space and the number of iterations of the Benders decomposition algorithm, we add to the master problem the following superset and subset cuts. These cuts help reduce the solution space of the master problem by limiting the number of feasible network configurations. Consequently, adding these constraints reduces the search space for the binary variables (Iyer and Grossmann 1998)

$$\sum_{(l,j,t)\in\mathcal{Y}^n_1}Y_{ljt}+Y_{ljt}\leq|\mathcal{Y}^n_1|,\quad\forall l\in\mathcal{L}^h,j\in\mathcal{J},t\in\mathcal{T}, \tag{59}$$

$$\sum_{(l,j,t)\notin\mathcal{Y}^n_1}Y_{ljt}+Y_{ljt}\geq 1,\quad\forall l\in\mathcal{L}^h,j\in\mathcal{J},t\in\mathcal{T}. \tag{60}$$

4.4.5. Heuristics Improvement Obtaining Good Solutions Before Convergence. The master problem is a mixed-integer linear program. This problem is difficult to solve; thus, obtaining an optimal solution for moderate sized networks is a challenging problem. The solutions obtained from solving the master problem in the initial iterations of the Benders algorithm are of low quality. This is mainly because initially, the master problem has not received much information about the subproblem. The quality of the solutions found improves as the algorithm progresses. Therefore, to reduce the running time of the algorithm, one can stop solving the master problem as soon as a feasible solution is found in the initial iterations of the Benders algorithm. As the algorithm progresses, we search for better solutions to the master problem.

To implement this, we initially set a large optimality gap when solving the master problem. This gap is gradually reduced as the algorithm progresses. The initial optimality gap is 5% and is reduced gradually to 1%.

Setting Branching Priorities. To accelerate the solution of the master problem, we set proper branching priorities for the decision variables of Z_{jkt}, Y_{lk}, and Y_{ljt}. Setting branching priorities provides CPLEX with the order in which the solver branches these variables. Numerical analysis indicates that branching on Z_{jkt} variables first followed by Y_{lk} and Y_{ljt} saves some computational time when solving the master problem.

4.5. A Hybrid Benders Based Rolling Horizon Algorithm

This approach combines the rolling horizon and accelerated Benders decomposition algorithms. The Benders decomposition algorithm is used to solve the subproblems created during the implementation of the rolling horizon algorithm.

When problems with sufficiently large-sized networks are solved using [RH], solving the first few subproblems created using CPLEX is difficult. However, as soon as the first few subproblems are solved, then the remaining subproblems can easily be solved by CPLEX. For this reason, when implementing the [RH] algorithm, we solve the first few subproblems using an accelerated Benders decomposition algorithm, and solve the remaining subproblems using CPLEX. The overall procedure, named [BRH], is described below:

Step 1. Initialize; set starting time period to $t^s_0=0$; set the length of time interval to N; set $s\leftarrow 1$.

Step 2. Solve the approximate subproblem [RH(s)] using accelerated Benders decomposition algorithm.

Step 3. If $t_0>|\mathcal{T}|$, then *Stop*; else, set $s\leftarrow s+1$, go to Step 2.

5. Computational Study and Managerial Insights

This section summarizes and interprets the results from the numerical study. The goal of this section is to test the performance of the algorithms proposed and draw important managerial insights about the supply chain. The case study is developed using data from the Southeast region of the United States.

5.1. Data Description

Biomass Supply. We have collected data about biomass availability from the following nine states: Mississippi, Alabama, Louisiana, Tennessee, Arkansas, Georgia, Florida, South Carolina, and North Carolina. The two main biomass feed stocks in this region are corn stover and forest residues. The biomass availability data are provided by the Bioenergy Knowledge Discovery Framework (KDF) database (KDF 2013). These

Figure 4. Biomass Distribution and Facility Locations

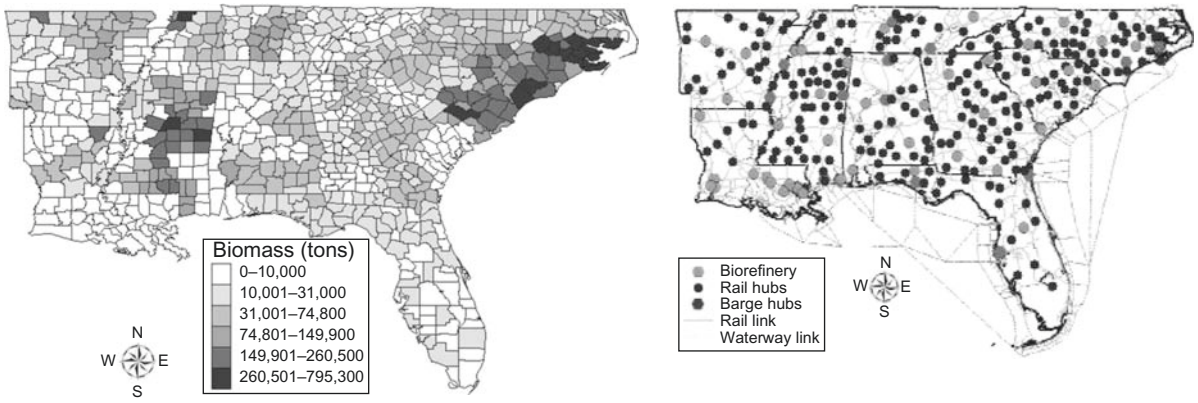

(a) Biomass distribution (b) Network representation

data were further processed by the INL to identify the amount of densified biomass available in this region. Figure 4(a) shows the distribution of densified biomass available for biofuel production in the Southeast. Altogether, 491 counties contributed to the collected data. The total amount of densified biomass available in the region is 29.35 million tons (MT) per year.

Biofuel Demand. The total fuel consumption in 2012 for the nine states listed above is 44.4 BGY (U.S. Energy Information Administration 2014). Based on the amount of biomass available in the region and considering a conversion rate of 72.6 gallons per MT, the total biofuel production in this region could be as high as 2.1 BGY. This amount corresponds to about 5% of the total fuel consumption in 2012. We consider this to be the total demand for cellulosic biofuel in the region. Recall that based on the proposed model, substitute products can be used to meet demand. The model allows this substitution to happen if the cost of producing biofuel exceeds the market price for substitute products. Therefore, setting the demand level high will not force the system to meet demand at any cost.

Counties with a population greater than 30,000 are considered as demand points in this study. Based on this criteria, we selected a total of 381 counties from the region. We assume that the distribution of the population in a particular region is a good indicator of the distribution of demand for biofuel. We use the centroid of the county as the point where demand occurs, and thus, where biofuel is to be delivered. In a year, the demand for gasoline typically rises in May and continues until September (U.S. Energy Information Administration 2013b), so the seasonality of demand in the biofuel demand data is incorporated in these formulations.

Investment Costs. We consider a total of 259 potential hub locations: 242 are rail ramps and 17 are inland/sea ports. Figure 4(b) presents the exact potential locations of these hubs and biorefineries. We consider a total of 44 potential biofuel plant locations. The annualized fixed cost for plants with a capacity of 45 million gallon per year (MGY) is set to \$159.4 million (You et al. 2012). This cost was estimated based on a project life of 20 years and an interest rate of 15%. We consider five different plant sizes: 20 MGY, 40 MGY, 60 MGY, 100 MGY, and 150 MGY. Wallace et al. (2005) estimate that doubling the size of the plant increases the investment cost by a factor of 1.6. We used this factor to calculate investment costs for the other biofuel plant sizes considered. The annualized fixed cost for a rail ramp of capacity 1.05 million ton per year (MTY) is equal to \$54,949/year (Mahmudi and Flynn 2006). We consider five different rail ramp capacities, where l=0.6 MTY, 0.8 MTY, 0.9 MTY, 1.05 MTY, and 1.20 MTY. These costs are estimated based on a lifetime of 30 years and a discount factor of 10%. The annualized fixed cost for an inland port of capacity 2.35 MTY is equal to \$306,000/year, which is derived from a study by Searcy et al. (2007). We consider five different port capacities, where l=1.0 MTY, 1.5 MTY, 1.75 MTY, 2.00 MTY, and 2.25 MTY. Although the actual fixed cost would vary by location, a common fixed cost is used as a reasonable approximation.

Transportation Costs. This study assumes that trucks are used to transport biomass from farms to multimodal facilities and biofuel plants. Trucks are also used to deliver biofuel to the market. Major cost components for truck transportation are obtained from a study by Parker et al. (2008), and these costs are summarized in Table 2.

Barge or rail can be used to deliver biomass at a multimodal facility. The unit transportation cost for barge shipments is estimated to be \$0.017/mile/ton (Gonzales, Searcy, and Eksioglu 2013). This cost is calculated assuming that a single tow boat pushes up to 15 barges, and each barge carries 1,500 tons of biomass.

Transportation costs by rail using CSXT and Burlington Northern Santa Fe (BNSF) Corporations are calculated using the following equations developed by

Table 2. Data About Truck Transportation

	Feedstock		Biofuel	
Item	Value	Unit	Value	Unit
Loading/unloading	5.0	$/wet ton	0.02	$/gallon
Time dependent	29.0	$/hr/truckload	32.0	$/hr/truckload
Distance dependent	1.20	$/mile/truckload	1.3	$/mile/truckload
Truck capacity	25	Wet tons/truckload	8,000	Gallons/truckload
Average travel speed	40	Miles/hour	40	Miles/hour

Gonzales, Searcy, and Eksioglu (2013). These equations represent the total transportation cost for a single rail car of capacity 100 tons. This cost is a function of the distance traveled (x_1)

$$Y_{\text{CSXT}} = 2{,}248 + 1.12x_1, \quad R^2_{\text{adj}}(\%) = 29.0; \quad p\text{-value}(\%) = 2E^{-22}, \tag{61}$$

$$Y_{\text{BNSF}} = 3{,}140 + 0.75x_1, \quad R^2_{\text{adj}}(\%) = 50.0; \quad p\text{-value}(\%) = 0.01. \tag{62}$$

The values \$2,248 and \$3,140 represent the fixed shipment cost per rail car, ξ_{jk}. The values \$1.12 and \$0.75 represent the unit transportation cost per mile. We multiply these costs with the travel distance between $j \in \mathcal{J}$ and $k \in \mathcal{K}$ to calculate c_{jk}.

We assume that a shipment is delivered from its source to its destination using the shortest path. Arc GIS Desktop 10 is used to create a transportation network, and then, this network identifies the shortest paths. The network includes existing railways; waterways; local, rural, urban roads; and major highways in the Southeast.

Estimating Disruption Probabilities. Failure probabilities at multimodal facilities are obtained from a study by Marufuzzaman et al. (2014). In developing these estimates, the authors consider the three major types of disasters that affect the Southeast: hurricanes, floods, and droughts. Based on National Hurricane Center data, the hurricane season starts in late August and ends in late September (National Hurricane Center 2013). Historically, the largest number of hurricanes was observed during the month of September. The U.S. Drought Monitor Center (2013a) provides historical data and weekly forecasts about the nationwide drought severity. The data for the period 2009 to 2013 indicates that the drought season starts in August and continues to January. The severity of droughts is greatest in September and October. We incorporated this information in the data set by assigning higher disruption probabilities during these months compared to other months of the season. Figure 5 presents the estimated disruption probabilities of the three disaster types collectively. These probabilities are presented for each candidate's multimodal facilities for the months of February (Figure 5(a)) and September (Figure 5(b)).

Summarizing the results from Figures 4 and 5, suggests that zone 1 has moderate biomass supply and faces moderate disruption risk; zone 2 has low biomass supply and faces low disruption risk; and zone 3 has high biomass supply and faces high disruption risk.

5.2. Experimental Results

We now discuss the results of our computational study. All of the algorithms are coded in General Algebraic Modeling System (GAMS) 24.2.1 (GAMS 2013) and are executed on a desktop computer with an Intel Core i7 3.5 GHz processor and 32 GB RAM. The optimization solver used is CPLEX 12.6.

5.2.1. Analyzing the Impact of Disruptions on the Supply Chain Performance. The goal of these numerical

Figure 5. Disruption Probability of Multimodal Facilities Estimated for Months (a) February and (b) September

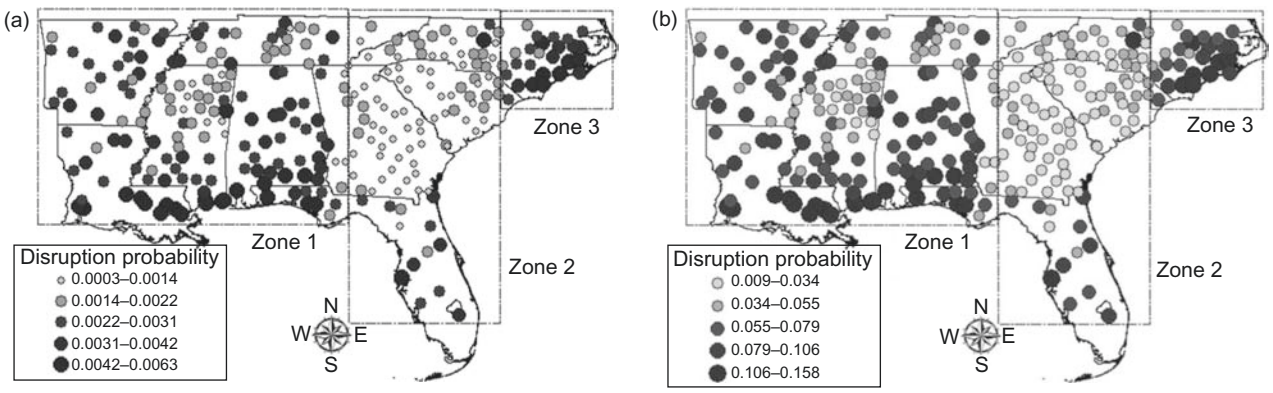

Figure 6. Impact of Disruption on System Performance

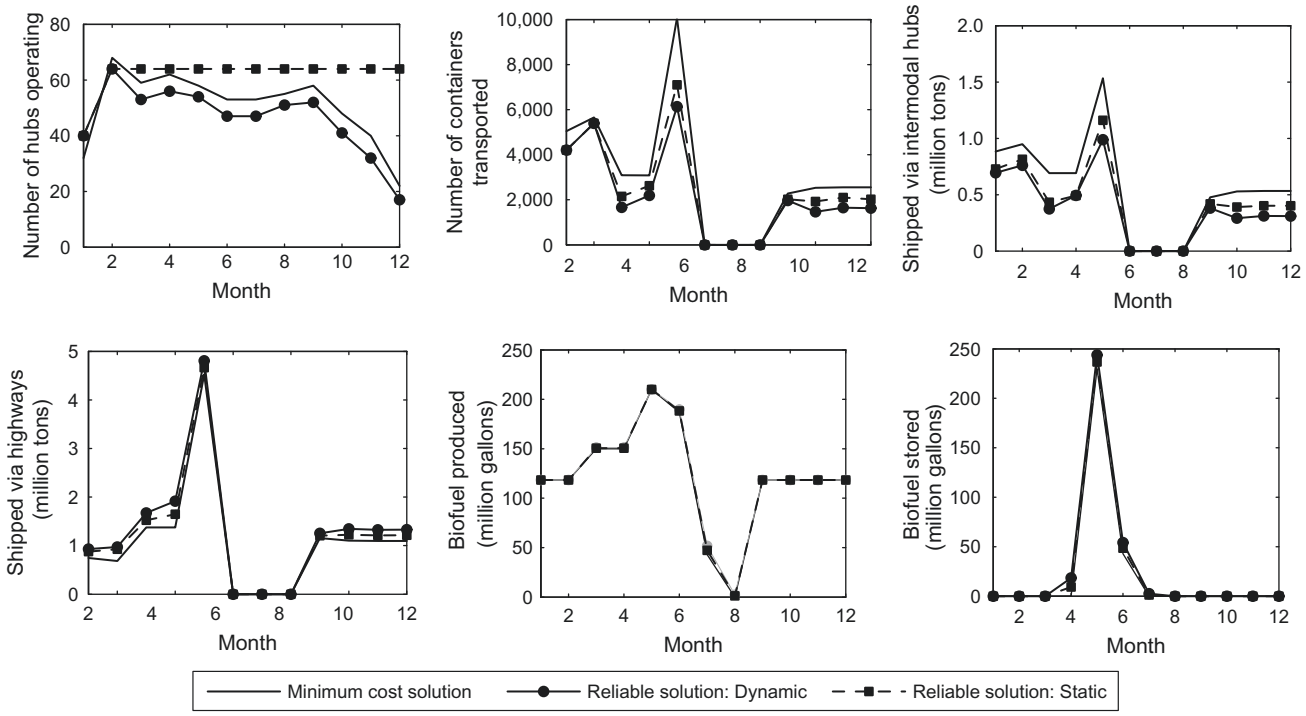

experiments is to evaluate the impact that disruptions have on the performance of the supply chain. We use a one-year planning horizon in which each period represents a month. Figure 6 presents the amount of biomass and biofuel produced, transported, and inventoried during each month of the planning horizon. Figure 6 also presents the number of hubs operating each month and the number of containers shipped. This information is essential to supporting strategic decisions and to guiding the planning of manpower and equipment during the year.

In the numerical experimentation, time $t=1$ corresponds to the month of July. Corn stover is typically harvested from September until November, which corresponds to periods $t=3$ to 5. Forest residues are harvested all year round except during the winter months of December to February ($t=6,7,8$) because of the heavy rains that make harvesting/collection challenging. To support the delivery of biomass to biofuel plants from September to November, additional hubs and containers are used. During this period, the amount shipped by trucks via highways also increases. The increase of truck transportation also occurs because weather conditions during the months of September and October correspond with the Southeast's hurricane season. This pick biomass production results in increased biofuel production and accumulation of biofuel inventory during periods 5 and 6 (November and December). Biomass transportation equals zero during the winter months. To satisfy demand for biofuels during these months, the inventories built up during September to November are depleted.

The three models compared above result from the same amount of biofuel produced and inventoried. The major difference between these models is the number of hubs operating. Almost the same number of hubs is open under each model in periods 1 and 2; however, the reliable and static model does not close these hubs during the months of low supply or during the hurricane season. Therefore, the annual costs related to hub operation are higher for the reliable and static model. This is one of the reasons why the unit delivery cost for such a system is so high—\$4.05 per gallon—compared to the \$3.86 and \$3.96 per gallon provided by the other two models (see Table 3). The minimum cost solution uses more hubs compared to reliable and dynamic solution because rail and barge transportation are more cost efficient than truck transportation. The reliable solution delivers less by barge during the hurricane season. The static and dynamic reliable solutions open three more biorefineries than the minimum cost solution. Building redundancies into the supply chain to hedge against disruptions is a common practice.

To quantify the benefits of designing reliable and dynamic supply chain systems, three different disruption scenarios are created. Table 3 summarizes the unit delivery cost of biofuel under each scenario. The first scenario assumes flooding of the Mississippi River. The second assumes flooding of the Tombigbee River, and the third scenario assumes a hurricane making landfall in North Carolina. The results indicate that in normal conditions, the minimum cost solution provides

Table 3. Comparison of Unit Cost Under Different Disrupted Scenarios

Scenarios	Min. cost ($/gallon)	Reliable and static hubs ($/gallon)	Reliable and dynamic ($/gallon)
1: Flooding of Mississippi River	4.91	4.78	4.48
2: Flooding of Tombigbee River	4.62	4.49	4.33
3: Hurricane in North Carolina	5.98	5.43	4.92
No disruption	3.86	4.05	3.96

the minimum delivery cost for this supply chain. The minimum cost model provides a solution that is 2.59% cheaper than the reliable and dynamic model and 4.92% cheaper than the reliable and static model. However, under disaster scenarios, the reliable and dynamic supply chain model outperforms both the minimum cost and reliable and static models. The minimum cost model is 2.65% to 9.20% more expensive than the reliable and static model and 6.28% to 17.73% more expensive than the reliable and dynamic model.

Figure 7 presents the impacts of disruptions on the supply chain network. Figure 7(a) shows the impact that disruptions would have on the supply chain resulting from solving the minimum cost model. Figure 7(b) presents the impacts of disruptions on the supply chain resulting from solving the reliable and static model, and Figure 7(c) presents the impacts of disruptions on the supply chain resulting from solving the reliable and dynamic model. The definition of the three model types are discussed in Section 3.2. Under scenario 1, three facilities would be impacted. Note the facilities we have circled in Figure 7 and labeled scenario 1. These facilities are inland ports along the Mississippi River. Disrupting these facilities would impact the operations of the biorefineries that they serve. Similarly, under scenario 2, one inland

Figure 7. Impacts of Disruption Scenarios on Network Configuration

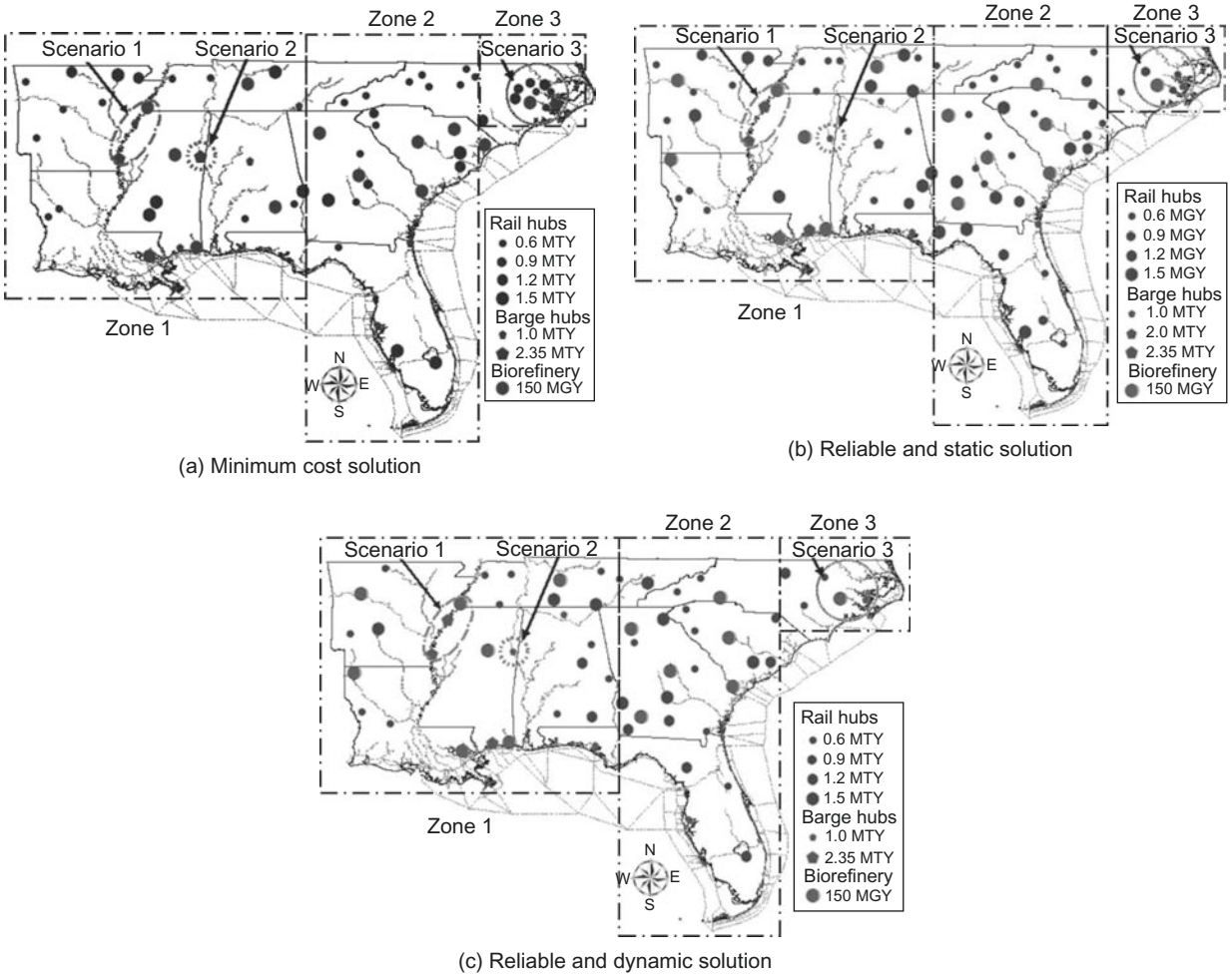

port along the Tombigbee River could be disrupted. To minimize the impact of disruptions, the capacity of this facility reduces from 2.35 MTY for the minimum cost solution to a 1.0 MTY for the reliable solution (Figure 7(b), the circled facility labeled scenario 2). In zone 3, a high-supply and high-risk area, the model locates a number of facilities to take advantage of the available biomass in the area. Under scenario 3, clearly the number of facilities that could be impacted by a disaster in North Carolina (zone 3) decreases drastically going from a minimum cost solution to a reliable solution. The minimum cost model relies heavily in using intermodal transportation to deliver the excess biomass to other plants. The reliable models open a smaller capacity port to deliver biomass and, in general, use fewer intermodal hubs. Fewer hubs are used for the dynamic than the static model.

5.2.2. Analyzing the Impact of the Biofuel Supply Chain on Highway Transportation. One of the challenges that the biofuel industry faces is delivering biomass to biofuel plants. Because of the high volume and low energy density of biomass, the volume of biomass required at a biofuel plant is large. Truck transportation—although more expensive as compared with other transportation modes—has been used extensively because of its availability and flexibility. Additionally, as the numerical analysis indicates, reliable supply chains use highways as a means of hedging against the risk of disruptions from natural disasters. Therefore, we think it is important to evaluate the increased shipment volumes in highways due to biomass transportation. Figure 8 summarizes some of the numerical results. The results presented compare the minimum cost model with the reliable and dynamic model, as well as the reliable and static model, as the amount of biomass available for delivery changes. The base for these comparisons uses the minimum cost solution to determine the amount of biomass to be shipped along highways. Note that in this experiment, we changed the total demand for biofuel in accordance with the change in feedstock supply scenarios.

Figure 8. Biomass Transported via Highways

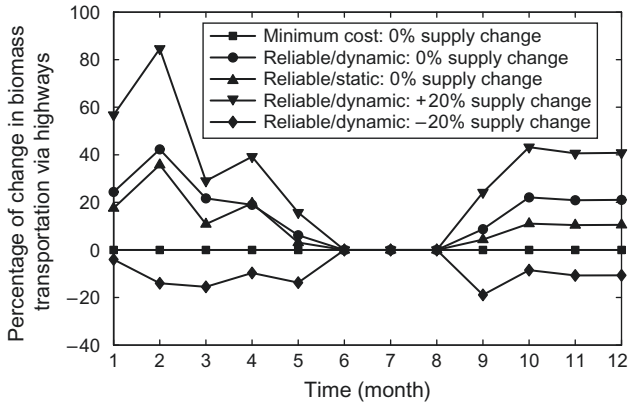

The results indicate that more biomass is shipped on highways under the reliable solutions than the minimum cost solutions; more biomass is shipped under the dynamic rather than static solutions. The amount shipped increases with the amount of biomass available. To deliver biomass available using minimum cost solution, on average, a total of 1,329 truck deliveries (trips) are required daily. Each truck on average travels 258 miles daily. This number increases to 1,543 truck deliveries daily for the reliable and dynamic model. Then, each truck on average travels 287 miles daily. This number further increases to 1,763 truck deliveries daily when biomass supply increases by 20% and the average number of miles traveled per truck is 304. The increase of truck transportation impacts the traffic on highways. Traffic congestion increases the noise around the communities where biofuel plants are located and impacts highway safety.

5.2.3. Analyzing the Impact of the Penalty Terms. Table 4 summarizes the results of our numerical analysis with respect to the penalty term. Based on these results, the penalty term could be very low (under \$3), could be very high (\$8 and above), or somewhere in between (\$3 to \$8). When the penalty is very high, the demand for biofuel is solely met via production (by using this supply chain). However, if the penalty is very small, then demand is met using other sources (not this supply chain).

Clearly, the problem is very easy when the penalty term is very low. In this case, the solution is simple; all of the demand is met using other sources (but this supply chain). As the penalty term increases, the running time of the algorithm naturally increases since different alternatives are evaluated. However, increasing the penalty term beyond \$8 has really little impact on the running time (for small or large plants). For example, going from \$8 to \$9, increases the running time 1.2% for the small capacity plant. The difficulty of the problem is not really impacted. The solutions we get from the penalty being 8, 9, and 10 are exactly the same (the amount of biofuel shipped, unsatisfied demand are equal). Total costs increase because the unmet demand is satisfied at a higher cost. To summarize, increasing the penalty cost beyond a certain value (\$8 for this problem) has only minor impacts on problem complexity and running time of the algorithm.

5.3. Analyzing the Performance of Solution Algorithms

This section presents our computational experience in solving the [LDR] model using the algorithms proposed in Section 4. We initially assess the performance of different accelerated techniques compared to the standard Benders decomposition algorithm (Table 6).

Table 4. Explaining the Impacts of Penalty Cost on System Performance[a, b]

	Capacity=250 MGY[c]				Capacity=200 MGY[c]			
Unit penalty cost ($)	Total system cost ($)	X_{kgt} (mil. gal.)	U_{gt} (mil. gal.)	Solution time (CPU sec)	Total system cost ($)	X_{kgt} (mil. gal.)	U_{gt} (mil. gal.)	Solution time (CPU sec)
10	1,106,228,910	250,000,000	23,122,891	322.4	1,431,228,910	200,000,000	73,122,891	342.2
9	1,083,106,019	250,000,000	23,122,891	321.6	1,358,106,019	200,000,000	73,122,891	338.6
8	1,059,983,128	250,000,000	23,122,891	318.5	1,284,983,128	200,000,000	73,122,891	334.5
7	1,046,820,341	247,154,256	25,968,635	311.1	1,217,969,949	198,254,368	74,868,523	322.8
6	1,043,350,384	238,154,785	34,968,106	282.4	1,151,774,176	194,785,268	78,337,623	302.7
5	1,018,847,086	231,178,246	41,944,645	294.3	1,090,741,338	183,248,745	89,874,146	299.3
4	996,412,096	192,158,936	80,963,955	288.7	1,014,748,454	155,486,221	117,636,670	279.1
3	820,997,164	3,256,982	269,865,909	221.7	831,943,156	25,148,966	247,973,925	234.9
2	546,245,782	0	273,122,891	47.5	546,245,782	0	273,122,891	56.1
1	273,122,891	0	273,122,891	44.2	273,122,891	0	273,122,891	51.4

[a]Solutions obtained by solving the accelerated Benders decomposition algorithm.
[b]Considered the following network size: $|\mathcal{H}|=100$, $|\mathcal{T}|=4$ to produce the results.
[c]Demand = 273,122,891 gallons.

Next, the performance of the rolling horizon algorithm is assessed and compared with CPLEX (Table 7). Finally, we compare the performance of all of the algorithms proposed with CPLEX (Table 8). The algorithms presented are terminated when at least one of the following conditions is met: (a) the optimality gap falls below a threshold value $\epsilon=0.01$, (b) the optimality gap is calculated as $\epsilon=|\text{UB}-\text{LB}|/\text{UB}$, or (c) the maximum time limit $t_{\max}=36{,}000$ (in CPU seconds) is reached. To terminate the Benders decomposition algorithm, we use an additional criterion: the maximum number of iterations $n=1{,}000$ is reached. The columns of the tables presented in this section provide the optimality gap (ϵ), the running time of the algorithm ($t_{\max}$), and the corresponding number of iterations (n). The best result is identified for each problem solved and is presented using boldface. Since a stopping criteria for the algorithm is $\epsilon \leq 1\%$, the algorithms are stopped when such a solution is found within the maximum time limit. The algorithm that gave the smallest running time is then highlighted. Otherwise, if such a quality solution is not found within the maximum time limit or number of iterations, the algorithm with the smallest optimality gap is highlighted. Table 5 summarizes the problem size considered for analyzing the performance of the solution algorithms.

For the first experiment, we consider nine levels for $|\mathcal{T}|=\{4,\ldots,12\}$ and three possible failure probabilities $\{q_j^t\}_{j\in\mathcal{J},t\in\mathcal{T}}=\{0.0,0.1,0.2\}$ to obtain 27 different problem instances. Table 6 summarizes the results from enhancements of the Benders decomposition algorithm. These enhancements are due to implementing the cuts described in Section 4.4. All of the algorithms presented in this table are further enhanced through the improvement techniques presented in Section 4.4.5. The total number of potential hubs for all of the problems presented in this table is 100. We do not present results from implementing the standard Benders decomposition algorithm, since when using this algorithm to solve the problems presented here, the

Table 5. Experimental Problem Sizes

$\lvert\mathcal{H}\rvert$	$\lvert\mathcal{I}\rvert$	$\lvert\mathcal{J}\rvert$	$\lvert\mathcal{K}\rvert$	$\lvert\mathcal{G}\rvert$	$\lvert\mathcal{T}\rvert$	$\lvert\mathcal{L}\rvert$	Binary variables	Integer variables	Continuous variables	Total variables	Total constraints
100	100	80	20	100	4	5	1,700	6,400	656,880	664,980	8,180
	100	80	20	100	8	5	3,300	12,800	1,313,760	1,329,860	16,340
	100	80	20	100	12	5	4,900	19,200	1,970,640	1,994,740	24,500
120	200	100	20	150	4	5	2,100	8,000	1,629,080	1,639,180	10,460
	200	100	20	150	8	5	4,100	16,000	3,258,160	3,278,260	20,900
	200	100	20	150	12	5	6,100	24,000	4,887,240	4,917,340	31,340
150	300	120	30	200	4	5	2,550	14,400	4,381,520	4,398,470	17,870
	300	120	30	200	8	5	4,950	28,800	8,763,040	8,796,790	35,710
	300	120	30	200	12	5	7,350	43,200	13,144,560	13,195,110	53,550
200	400	170	30	250	4	5	3,550	20,400	8,239,720	8,263,670	24,670
	400	170	30	250	8	5	6,950	40,800	16,479,440	16,527,190	49,310
	400	170	30	250	12	5	10,350	61,200	24,719,160	24,790,710	73,950
259	491	220	39	267	4	5	4,595	34,320	16,971,372	17,010,287	39,519
	491	220	39	267	8	5	8,995	68,640	33,942,744	34,020,379	78,999
	491	220	39	267	12	5	13,395	102,960	50,914,116	51,030,471	118,479

Table 6. Summary of Results from Implementing Enhancements of Benders Decomposition Algorithm

		Benders+PO			Benders+PO+KI			Benders+PO+KI+LC			All cuts		
$\lvert\mathcal{T}\rvert$	q_j^t	ϵ	$t_{\max}$	n	ϵ	$t_{\max}$	n	ϵ	$t_{\max}$	n	ϵ	$t_{\max}$	n
4	0.0	0.81	383.6	28	0.81	348.7	25	0.92	335.1	24	0.75	**73.2**	6
	0.1	0.77	322.8	24	0.94	301.4	22	0.77	287.1	21	0.76	**73.7**	6
	0.2	0.74	266.9	20	0.68	244.6	18	0.85	273.7	20	0.76	**73.8**	6
5	0.0	0.95	513.4	29	0.92	470.3	26	0.97	429.4	24	0.91	**90.7**	6
	0.1	0.52	461.1	26	0.91	451.5	26	0.78	431.5	24	0.92	**91.5**	6
	0.2	0.94	297.6	18	0.95	342.7	20	0.85	344.5	20	0.91	**91.8**	6
6	0.0	0.91	704.7	34	0.97	566.4	26	0.82	565.2	26	0.05	**104.5**	5
	0.1	0.77	532.5	26	0.87	524.8	24	0.91	487.2	23	0.62	**105.9**	5
	0.2	0.61	394.1	21	0.94	385.9	18	0.98	364.2	17	0.52	**106.1**	5
7	0.0	0.97	731.4	30	0.74	740.7	29	0.29	723.1	28	0.92	**169.2**	7
	0.1	0.91	688.2	26	0.89	711.8	28	0.48	687.5	26	0.89	**170.2**	7
	0.2	0.99	486.2	20	0.84	614.1	27	0.38	520.4	20	0.87	**169.9**	7
8	0.0	0.78	816.6	29	0.60	894.9	30	0.89	916.5	31	0.27	**204.1**	8
	0.1	0.87	998.1	37	0.88	989.4	35	0.91	929.1	32	0.21	**223.0**	8
	0.2	0.99	701.4	25	0.78	616.0	21	0.77	523.0	18	0.22	**226.6**	8
9	0.0	0.97	1,085.5	34	0.36	1,118.2	33	0.97	1,073.1	30	0.91	**219.1**	7
	0.1	0.94	1,178.4	37	0.89	1,194.1	35	0.91	1,101.4	31	0.93	**222.4**	7
	0.2	0.87	761.5	24	0.78	724.8	22	0.79	660.7	20	0.89	**228.0**	7
10	0.0	0.98	1,400.4	39	0.99	1,400.6	38	0.94	1,164.7	31	0.84	**320.1**	9
	0.1	0.96	1,480.6	37	0.94	1,311.8	34	0.97	1,308.1	35	0.78	**321.8**	9
	0.2	0.97	1,105.8	31	0.86	882.0	24	0.91	779.2	21	0.92	**324.8**	9
11	0.0	0.97	2,337.6	56	0.97	2,340.1	51	0.96	1,837.6	39	0.98	**727.1**	18
	0.1	0.94	1,752.8	38	0.94	1,344.5	32	0.94	1,322.3	31	0.94	**743.2**	18
	0.2	0.89	1,218.4	32	0.97	1,175.1	29	0.96	1,167.4	28	0.97	**717.7**	16
12	0.0	0.97	2,427.9	56	0.95	2,354.0	49	0.98	2,527.6	54	0.95	**1,216.9**	26
	0.1	0.98	1,778.8	39	0.97	1,545.9	33	0.87	1,524.1	33	0.89	**1,028.6**	23
	0.2	0.97	1,268.8	29	0.96	1,180.3	27	0.95	1,368.1	29	0.94	**756.2**	16
Average		0.89	966.5	31.3	0.86	917.6	29.0	0.84	876.0	27.3	0.76	**325.9**	9.7

Note. PO, Pareto-optimal cuts; KI, knapsack inequalities; LC, logistics constraints; all cuts, cuts including Pareto-optimal cuts, knapsack inequalities, logistics constraints, and integer cuts.

solutions found within 1,000 iterations had an optimality gap of at least 20%. The results indicate that implementing the cuts presented in Section 4.4 substantially improves the performance of the Benders algorithm. The results from *all cuts* Benders decomposition algorithm—which in addition to Pareto optimal, knapsack, and logistics cuts uses the integer cuts—indicate a running time improved 1.68 times compared to the accelerated Benders decomposition algorithm without these integer cuts. Results indicate that incorporating the integer cuts significantly reduces the average number of iterations required by the accelerated Benders decomposition algorithm compared to implementations of the accelerated Benders decomposition algorithm without the integer cuts. Note that, because of the possibility of cutting off an optimal solution, we turn off the integer cuts when the optimality gap of the Benders decomposition algorithm reaches below 5% and rely on Pareto-optimal cuts, logistics constraints, and knapsack inequalities to reach the optimality gap to a prespecified tolerance gap (ϵ). The number of iterations (n) reported in Tables 6 and 8 represents the number of cuts required to reach an optimality gap below a prespecified tolerance ϵ (i.e., 1.0%). We do not generate feasibility cuts since the solution to the subproblem is always feasible because of constraints (35). Since the integer cuts, knapsack inequalities, and Pareto-optimal cuts are added from the second iteration, we generate in total $n-1$ of these cuts in solving model [LDR] using the Benders decomposition algorithm.

Table 7 compares the computational results of solving the [LDR] model using the rolling horizon algorithm and CPLEX. The number of potential hubs and time periods differ from one problem to another. The performance of the algorithm is investigated as the values of these two problem parameters change because they greatly impact problem size, and consequently, the running time of the algorithm. Each subproblem created during the implementation of the rolling horizon algorithm is solved using CPLEX. We experiment with the stopping criteria used to stop CPLEX when solving these subproblems. We investigate the performance of the [RH] algorithm when the optimality gap used for subproblems equals 1% and 2%. Increasing the gap from 1% to 2% reduces the overall running time of the [LDR] algorithm. Another

Table 7. Summary of Results from Implementing the RH Algorithm and CPLEX

			CPLEX		RH 1.0%		RH 2.0%	
$\lvert\mathcal{H}\rvert$	$\lvert\mathcal{T}\rvert$	q_j^t	ϵ	$t_{\max}$	ϵ	$t_{\max}$	ϵ	$t_{\max}$
100	10	0.0	**0.99**	686.5	1.17	190.8	1.30	120.8
		0.1	**0.99**	454.4	1.04	256.4	1.41	143.1
	12	0.0	**0.99**	1,626.2	1.17	480.8	1.45	249.0
		0.1	0.95	1,865.7	0.91	**658.6**	1.44	288.7
120	10	0.0	0.75	9,648.8	0.30	**1,477.6**	1.59	722.2
		0.1	0.21	10,110.4	0.29	**1,913.3**	1.23	889.5
	12	0.0	0.72	11,748.1	0.91	**3,161.6**	1.71	1,121.5
		0.1	0.82	12,723.7	0.86	**4,123.2**	1.62	1,485.5
140	10	0.0	5.65	36,000.0	**2.08**[a]	10,847.8	2.18	1,247.8
		0.1	5.15	36,000.0	**2.09**[a]	11,623.3	2.12	2,023.3
	12	0.0	12.69	36,000.0	**3.04**[a]	12,427.3	**3.04**[a]	12,427.3
		0.1	12.86	36,000.0	**3.29**[a]	12,716.8	**3.29**[a]	12,716.8
Average			3.56	16,072.0	**1.f43**	4,989.8	1.86	2,786.3

[a]Unable to solve the first subproblem within the specified optimality gap within 10,800 CPU seconds.

criterion used to stop CPLEX is a maximum running time of 10,800 CPU seconds.

Results indicate that the benefits of the [RH] algorithm over CPLEX are evident as the problem size increases, either because of increasing the number of potential hubs or the number of time periods considered in this problem. Our experience with [RH] algorithm indicates that solving the first subproblem is difficult, and therefore time consuming. Stopping CPLEX when $\epsilon=1\%$ or 2%—although it helped some—did not have a great impact on reducing the time it took to solve this subproblem. Because the first subproblem is challenging, CPLEX fails to solve it as the number of potential hubs increases. Note the results for $|\mathcal{H}|=140$, $|\mathcal{T}|=10$ and 12 in Table 7. Once the first subproblem is solved, the rest can be solved quickly.

Table 8 presents the results from solving the [LDR] model using the algorithms proposed in this paper. The problems solved differ by the number of potential hub locations considered, the length of planning horizon, and thus, the problem size. We do not present results for problems with $|\mathcal{H}|<100$. For those problems, CPLEX provided the best results and outperformed the algorithms presented here. The benefits of using the algorithms we develop becomes evident as the problem size increases, which is the case when $|\mathcal{H}|\geq 100$.

Results indicate that, in 33 out of 36 problem instances solved, the accelerated Benders decomposition algorithm provides solutions with an optimality gap less than 1.0% within the specified time limit. The benefits of using the greedy [RH] and the hybrid Benders based [RH] algorithms can clearly be seen as the problem size increases. Both algorithms are able to find high-quality solutions within relatively small computational time. The overall average optimality gap for the greedy [RH] algorithm is 1.82%, with only one out of 36 problem instances exceeding 5.0% gap. The overall average optimality gap for the hybrid Benders based [RH] algorithm is 1.41%. The largest three problem instances presented in Table 8 show noticeable improvements of both algorithms in terms of solution quality and running time as compared to other solution approaches. Overall, both the greedy [RH] and the hybrid Benders-based [RH] algorithms seem to offer high-quality solutions consistently within the experimental range.

6. Conclusion

This paper presents an MIP model that helps supply chain managers to design cost-efficient and reliable supply chain networks for biomass delivery to biofuel plants and biofuel delivery to markets. The proposed inbound supply chain of biofuel plants has a multimodal facility structure. Multimodal facility networks are typically used for high-volume, long-haul transportation of bulk products. Such a network design facilitates the transportation of biomass in a cost-efficient manner. This system relies on using inland ports, sea ports, and rail stations for the delivery of biomass by rail and barge between multimodal facilities. Activities at ports could be disrupted by natural disasters, such as floods, hurricanes, and droughts. Therefore, considering the risks associated with these disruptions when designing biofuel supply chains makes sense.

The model we propose captures supply chain uncertainties due to natural disruptions and biomass seasonality since these factors impact the performance of biofuel supply chains. To handle these uncertainties efficiently, the model proposes to adjust short-term and midterm supply chain decisions dynamically under disaster scenarios. Numerical results indicate that such an approach results in cost savings in the supply chain.

The MIP model proposed is an extension of the capacitated facility location problem, and therefore, it is an $\mathcal{NP}$-hard problem. To solve this problem, we propose the following solution approaches: a rolling horizon algorithm, a greedy rolling horizon algorithm, an accelerated Benders decomposition algorithm, and a hybrid Benders-based rolling horizon algorithm. We test the performance of these algorithms in a case study we build using data from the Southeast United States. Numerical results indicate that the accelerated Benders and the hybrid algorithms outperform the rest. Although the accelerated Benders provides solutions of high quality, the hybrid algorithm provides good quality solutions in a reasonable amount of time. For very large problem instances, the hybrid algorithm outperforms the accelerated Benders decomposition algorithm. For these large problem instances CPLEX

Table 8. Comparison of Different Solution Approaches

			CPLEX		RH-algorithm		Greedy RH		Accelerated Benders[c]			RH-Benders	
$\|\mathcal{H}\|$	$\|\mathcal{T}\|$	q_j^t	ϵ	t_{max}	ϵ	t_{max}	ϵ	t_{max}	ϵ	t_{max}	n	ϵ	t_{max}
100	4	0.0	0.72	64.8	0.72	47.9	0.77	**30.8**	0.75	73.2	6	0.88	106.7
		0.1	0.51	120.7	1.01	107.8	1.17	40.9	0.76	**73.7**	6	0.58	109.1
		0.2	0.46	127.4	1.60	119.9	1.14	37.2	0.76	**73.8**	6	0.81	120.1
	8	0.0	0.66	**109.8**	1.22	96.6	1.14	90.2	0.27	204.1	8	1.05	174.0
		0.1	0.75	195.9	0.97	**166.6**	1.17	104.7	0.21	223.0	8	0.92	169.1
		0.2	0.74	195.8	1.18	223.3	1.15	95.8	0.22	226.6	8	0.92	**173.1**
	12	0.0	0.99	1,626.2	1.17	480.8	1.26	299.2	0.95	**1,216.9**	26	1.10	449.6
		0.1	0.95	1,865.7	0.91	**658.6**	1.34	219.1	0.89	1,028.6	23	1.07	423.8
		0.2	0.98	1,368.1	1.09	547.7	1.65	236.5	0.94	756.2	16	0.61	**406.1**
150	4	0.0	5.40	36,000.0	0.52	1,015.6	0.66	**378.3**	0.91	559.5	8	0.55	442.2
		0.1	5.30	36,000.0	1.12	2,066.1	1.17	712.2	0.94	**563.8**	8	1.22	747.5
		0.2	4.98	36,000.0	1.55	2,436.2	1.41	615.8	0.93	**561.3**	8	0.82	698.7
	8	0.0	7.47	36,000.0	2.59	11,203.6	0.61	1,091.1	0.97	2,393.4	14	0.74	**1,017.2**
		0.1	4.16	36,000.0	2.39	7,234.5	1.31	1,798.5	0.88	**2,428.3**	15	1.12	1,121.2
		0.2	4.58	36,000.0	1.53	6,940.0	1.69	2,308.5	0.79	**2,210.2**	13	1.67	1,160.3
	12	0.0	16.70	36,000.0	3.35	12,830.3	0.55	2,830.9	0.87	9,758.8	37	0.85	**2,814.5**
		0.1	17.02	36,000.0	3.13	12,210.2	0.55	**2,449.8**	0.96	9,112.5	36	1.18	2,842.1
		0.2	15.70	36,000.0	5.97	11,035.6	0.63	**2,367.4**	0.86	9,142.6	36	1.22	2,902.8
200	4	0.0	6.74	36,000.0	2.19	1,862.0	2.23	726.2	0.39	**799.0**	6	1.10	1,132.6
		0.1	6.82	36,000.0	2.35	3,247.6	2.22	1,125.8	0.76	**822.1**	6	1.65	1,215.6
		0.2	9.09	36,000.0	2.23	3,349.4	1.99	1,014.9	0.49	**963.8**	7	1.70	1,255.5
	8	0.0	10.67	36,000.0	3.48	12,733.3	2.89	1,974.3	0.97	**2,640.3**	9	1.83	1,805.3
		0.1	10.75	36,000.0	3.02	8,477.9	2.75	2,122.5	0.84	**2,998.6**	10	2.04	1,600.2
		0.2	10.39	36,000.0	4.60	8,847.6	2.69	2,899.4	0.69	**2627.8**	9	1.72	1,578.8
	12	0.0	19.89	36,000.0	5.51	13,581.1	5.03	4,294.4	0.11	**14,357.9**	27	2.57	4,693.0
		0.1	17.57	36,000.0	5.67	13,612.5	4.49	4,688.7	0.23	**14,412.8**	27	2.00	4,585.5
		0.2	13.96	36,000.0	5.19	13,771.5	3.92	4,442.9	0.49	**14,222.2**	27	1.99	4,492.2
259	4	0.0	11.75	36,000.0	1.75	12,094.3	1.10	3,531.1	0.94	**10,413.5**	23	2.00	3,780.3
		0.1	15.04	36,000.0	2.37	12,174.6	1.65	3,811.5	0.89	**11,254.2**	24	1.85	3,752.1
		0.2	13.04	36,000.0	2.53	12,221.7	1.63	4,289.4	0.84	**11,294.7**	24	1.58	3,698.5
	8	0.0	12.39	36,000.0	2.33	15,121.7	0.97	**7,214.5**	0.86	30,180.0	28	1.75	6,592.6
		0.1	15.80	36,000.0	3.13	15,249.7	2.22	7,415.8	0.97	**28,322.4**	27	1.91	6,789.4
		0.2	13.89	36,000.0	4.59	15,987.2	2.66	7,445.9	0.94	**28,111.2**	27	2.12	6,994.2
	12	0.0	*mem*[a]	*mem*	*n.a.*[b]	*n.a.*	1.58	15,988.9	17.22	36,000.0	18	0.99	**14,155.4**
		0.1	*mem*	*mem*	*n.a.*	*n.a.*	2.37	16,289.4	14.61	36,000.0	19	**1.95**	14,478.6
		0.2	*mem*	*mem*	*n.a.*	*n.a.*	3.82	16,672.6	13.89	36,000.0	19	**2.75**	14,214.9
Average			8.36	26,354	2.51	7,025.8	1.82	3,379.3	1.94	8,945.2	17	**1.41**	**3,130.4**

[a]Runs out of memory.
[b]Unable to find an integer feasible solution within the time limit.
[c]Accelerated Benders decomposition includes Pareto-optimal cuts, knapsack inequalities, logistics constraints, and integer cuts.

runs out of memory, and the rolling horizon algorithm fails to find an integer-feasible solution within the time limit.

We conducted extensive numerical analyses to provide insights about the advantages of using the model proposed to optimize the performance of the supply chain. We compare our model to a minimum cost model, with the goal of minimizing total costs, to a reliable but static model, with the goal minimizing expected costs under normal and disruption scenarios. Under normal conditions, the minimum cost model outperforms the rest. However, under disaster scenarios, the reliable and dynamic supply chain model proposed in this paper outperforms the minimum cost and reliable and static models. The minimum cost model is 2.65% to 9.20% more expensive than the reliable and static model and 6.28% to 17.73% more expensive than the reliable and dynamic model.

This work can be extended in several ways. In this study we assume that intermodal hubs fail independently. This is mainly because the hubs selected in a supply chain for shipment consolidations and deconsolidations would typically be located far away from one another, and therefore, the chances that these hubs are impacted by the same disasters are very small. We also assume that failure probabilities are temporar-

ily independent. This is mainly because we assume the length of a time period to be a month. Thus, the chances that the impacts of a disaster span more than a month are small. We make this assumption because the model proposed here integrates strategic and planning (rather than day-to-day) decisions. However, in real life, disasters have more complex failure patterns. We identify as future work extensions of the current model to consider time- and space-dependent probabilities. Furthermore, our work can be extended to consider congestions caused by multimodal facility failure during disruption. These issues will be addressed in future studies.

Acknowledgments

The authors are grateful to the reviewers whose insightful comments helped to improve the quality of this paper. This support is gratefully acknowledged.

Appendix

Table A.1. Mississippi River Flooding History Between 1900–2011

Name of the flood	Year	Most affected months
Great Mississippi flood of 1927	1927	May–December
Great flood of 1937	1937	January–February
Flood of 1945	1945	March–May
Mississippi flood of 1973	1973	March–May
Flood of 1975	1975	April
Flood of 1979	1979	April
Lower Mississippi flood	1983	May–June
Great Mississippi and Missouri Rivers flood	1993	April–October
Flood of 2002	2002	April
Flood of 2008	2008	April–May
Great Mississippi flood of 2011	2011	April–May

Source. Trotter et al. (2011).

References

An H, Wilhelm WE, Searcy SW (2011) A mathematical model to design a lignocellulosic biofuel supply chain system with a case study based on a region in central Texas. *Bioresource Tech.* 102:7860–7870.

An Y, Zhang Y, Zeng B (2015) The reliable hub-and-spoe design problem: Models and algorithms. *Transportation Res. Part B* 77: 103–122.

Balasubramanian J, Grossmann I (2004) Approximation to multistage stochastic optimization in multiperiod batch plant scheduling under demand uncertainty. *Indust. Engrg. Chemistry Res.* 43:3695–3713.

Benders JF (1962) Partitioning procedures for solving mixed-variables programming problems. *Numerische Mathematik* 4: 238–252.

Bioenergy Knowledge Discovery Framework (KDF) (2013). https://bioenergykdf.net/taxonomy/term/1036.

Campbell JF (1990) Locating transportation terminals to serve an expanding demand. *Transportation Res. Part B* 3:173–192.

Chen C-W, Fan Y (2012) Bioethanol supply chain system planning under supply and demand uncertainities. *Transportation Res. Part E* 48:150–164.

Contreras I, Cordeau J, Laporte G (2011) The dynamic uncapacitated hub location problem. *Transportation Sci.* 45:18–32.

Credeur MJ (2011) FedEx in Paris disrupted as workers walk out. *Bloomberg* (May 13), http://www.bloomberg.com/news/2011-05-13/fedex-s-paris-hub-disrupted-as-union-workers-walk-off-job-1-.html.

Cui T, Ouyang Y, Shen ZM (2010) Reliable facility location under the risk of disruptions. *Oper. Res.* 58:998–1011.

Daskin MS (1982) Application of an expected covering model to emergency medical service system design. *Decision Sci.* 13: 416–439.

Daskin MS (1983) A maximum expected covering location model: Formulation, properties and heuristic solution. *Transportation Sci.* 17:48–70.

Drezner Z (1987) Heuristic solution methods for two location problems with unreliable facilities. *J. Oper. Res. Soc.* 38:509–514.

Eksioglu SD, Acharya A, Leightley LE, Arora S (2009) Analyzing the design and management of biomass-to-biorefinery supply chain. *Comput. Indust. Engrg.* 57:1342–1352.

Eksioglu SD, Palak G, Mondala A, Greenwood A (2013) Supply chain designs and management for biocrude production via wastewater treatment. *Environ. Progress Sustainable Energy* 32: 139–147.

Eksioglu SD, Li S, Zhang S, Sokhansanj S, Petrolia D (2010) Analyzing impact of intermodal facilities on design and management of biofuel supply chain. *Transportation Res. Record* 2191:144–151.

Fischetti M, Lodi A (2003) Local branching. *Math. Programming* 98: 23–47.

General Algebraic Modeling System (GAMS) (2013) http://www.gams.com/.

Ghaderi A, Boland N, JabalAmeli MS (2012) Exact and heuristic approaches to the budget-constrained dynamic uncapacitated facility location-network design problem. Centre for Optimal Planning and Operations, University of Newcastle, Newcastle, UK, http://www.optimization-online.org/DB-FILE/2012/02/3336.pdf.

Gill V (2010) Lessons to be learned from Haiti's tsunami. *BBC News* (February 25), http://news.bbc.co.uk/2/hi/science/nature/8536561.stm.

Gonzales D, Searcy EM, Eksioglu SD (2013) Cost analysis for high-volume and long-haul transportation of densified biomass feedstock. *Transportation Res. Part A* 49:48–61.

Hess JR, Wright TC, Kenney LK, Searcy ME (2009) Uniform-format solid feedstock supply system: A commodity-scale design to produce an infrastructure-compatible bulk solid from lignocellulosic biomass. Technical report, INL/EXT-09-15423, Idaho National Laboratory, Idaho Falls, ID, http://www.inl.gov/technicalpublications/Documents/4408280.pdf.

Hinojosa Y, Kalcsics J, Nickel S, Puerto J, Velten S (2008) Dynamic supply chain design with inventory. *Comput. Oper. Res.* 35: 373–391.

Huang Y, Chen CW, Fan Y (2010) Multistage optimization of the supply chains of biofuels. *Transportation Res. Part E* 46:820–830.

Huang Y, Fan Y, Chen C-W (2014) An integrated biofuel supply chain against feedstock seasonality and uncertainty. *Transportation Sci.* 48:540–554.

Iyer RR, Grossmann IE (1998) A bilevel decomposition algorithm for long-range planning of process networks. *Indust. Engrg. Chemistry Res.* 37:474–481.

Kang S, Onal H, Ouyang Y, Scheffran J, Tursun D (2010) Optimizing the biofuels infrastructure: Transportation networks and biorefinery locations in Illinois. Khanna M, Scheffran J, Zilberman D, Dinar A, Zilberman D, eds. *Handbook of Bioenergy Economics and Policy*, Vol. 33 (Springer, New York), 151–173.

Kim J, Realff MF, Lee JH (2011) Optimal design and global sensitivity analysis of biomass supply chain networks for biofuels under uncertainty. *Comput. Chemical Engrg.* 35:1738–1751.

Kostina AM, Guillen-Gosalbeza G, Meleb FD, Bagajewiczc MJ, Jimeneza L (2011) A novel rolling horizon strategy for the strategic planning of supply chains. Application to the sugar cane industry of Argentina. *Comput. Chemical Engrg.* 35: 2540–2563.

Li Q, Zeng B, Savachkin A (2013) Reliable facility location design under disruptions. *Comput. Oper. Res.* 40:901–909.

Li X, Ouyang Y (2010) A continuous approximation approach to reliable facility location design under correlated probabilistic disruptions. *Transportation Res. Part B* 44:535–548.

Li X, Peng F, Bai Y, Ouyang Y (2011) Effects of disruption risks on biorefinery location design: Discrete and continuous models. *Proc. 90th TRB Annual Meeting, Washington, DC.* https://trid.trb.org/view.aspx?id=1091311.

Magnanti TL, Wong RT (1981) Acclerating Benders decomposition: Algorithmic enhancement and model selection criteria. *Oper. Res.* 29:464–484.

Mahmudi H, Flynn P (2006) Rail vs. truck transport of biomass. *Appl. Biochemistry Biotechnology* 129:88–103.

Marufuzzaman M, Eksioglu SD, Li X, Wang J (2014) Analyzing the impact of intermodal-related risk to the design and management of biofuel supply chain. *Transportation Res. Part E* 69: 122–145.

Melo MT, Nickel S, Saldanha da Gama F (2005) Dynamic multicommodity capacitated facility location: A mathematical modeling framework for strategic supply chain planning. *Comput. Oper. Res.* 33:181–208.

Mouawad J (2005) Katrina's shock to the system. *New York Times* (September 4), http://www.nytimes.com/2005/09/04/business/04oi.html?pagewanted=all&-r=0.

National Hurricane Center (2013) Hurricane season summaries and reports. http://www.nhc.noaa.gov.

National Oceanic and Atmospheric Administration (2005) Hurricane Katrina. http://www1.ncdc.noaa.gov/pub/data/extremeevents/specialreports/Hurricane-Katrina.pdf.

Oosterhuis M, Molleman E, Vaart TVD (2005) Multilevel issues in supply chain management. Oosterhuis M, Molleman E, Vaart TVD, eds. *Research Methodologies in Supply Chain Management* (Physica-Verlag HD, Heidelberg, Germany), 283–297.

Pacific Northwest National Laboratory (2013) Looking back at the August 2003 blackout. http://eioc.pnnl.gov/research/2003blackout.stm.

Papadakos N (2008) Practical enhancements to the Magnanti-Wong method. *Oper. Res. Lett.* 36:444–449.

Parker N, Tittmann P, Hart Q, Lay M, Cunningham J, Jenkins B, Nelson R, Skog K, Milbrandt A, Gray E, Schmidt A (2008) Strategic assessment of bioenergy development in the west: Spatial analysis and supply curve development. Report, Western Governors' Association, University of California, Davis.

Peng P, Snyder LV, Lim A, Lio Z (2011) Reliable logistics networks design with facility disruptions. *Transportation Res. Part B* 45: 1190–1211.

Polson J (2011) BP oil still ashore one year after end of Gulf spill. *Bloomberg* (July 15), http://www.bloomberg.com/news/2011-07-15/bp-oil-still-washing-ashore-one-year-after-end-of-gulf-spill.html.

Renewable Fuels Association (2013) Monthly U.S. fuel ethanol production/demand. http://ethanolrfa.org/pages/monthly-fuel-ethanol-production-demand.

Roy TJV (1986) A cross decomposition algorithm for capacitated facility location. *Oper. Res.* 34:145–163.

Santoso T, Ahmed S, Goetschalckx M, Shapiro A (2005) A stochastic programming approach for supply chain network design under uncertainty. *Eur. J. Oper. Res.* 167:96–115.

Searcy E, Flynn P, Ghafoori E, Kumar A (2007) The relative cost of biomass energy transport. *Appl. Biochemistry Biotechnology* 137–140:639–652.

Shen JM, Zhan RL, Zhang J (2011) The reliable facility location problem: Formulations, heuristics, and approximation algorithms. *INFORMS J. Comput.* 23:470–482.

Snyder LV, Daskin MS (2005) Reliability models for facility location: The expected failure cost case. *Transportation Sci.* 39:400–416.

Snyder LV, Scaparra MP, Daskin MS, Church RL (2006) Planning for disruptions in supply chain networks. Johnson MP, Norman B, Secomandi N, eds. *TutORials in Operations Research* (INFORMS, Hanover, MD), 234–257.

State Climate Office at North Carolina (2012) Total storms affecting NC by decades within 150 miles (1851–2012). http://www.nc-climate.ncsu.edu/climate/hurricanes/statistics.php.

Trotter PS, Johnson GA, Ricks R, Smith DR (2011) Floods on the lower Mississippi: An historical economic overview. http://www.srh.noaa.gov/topics/attach/html/ssd98-9.htm.

U.S. Drought Monitor (2013a) Percent area in U.S. drought monitor categories. http://www.droughtmonitor.unl.edu/DataArchive/Tables.aspx.

U.S. Drought Monitor (2013b) U.S. drought monitor data archive. http://www.droughtmonitor.unl.edu/DataArchive.aspx.

U.S. Energy Information Administration (2013a) Monthly biodiesel production report. http://www.eia.gov/biofuels/biodiesel/production/.

U.S. Energy Information Administration (2013b) U.S. gasoline demand. http://www.eia.gov/oog/info/twip/twip-gasoline.html.

U.S. Energy Information Administration (2014) State Energy Data System (SEDS): 2012 (Updates). http://www.eia.gov/state/seds/seds-data-fuel.cfm?sid=US.

U.S. Environmental Protection Agency (2007) Renewable fuels: Regulations and standards. http://www.epa.gov/otaq/fuels/renewablefuels/regulations.htm.

Uster H, Agrahari H (2011) A Benders decomposition approach for a distribution network design problem with consolidation and capacity considerations. *Oper. Res. Lett.* 39:138–143.

Wallace R, Ibsen K, McAloon A, Yee W (2005) Feasibility study for co-locating and integrating ethanol production plants from corn starch and lignocellulose feedstocks. Technical report, NREL/TP-510-37092, USDA/USDOE/NREL, Revised Edition, Golden, CO.

Wang X, Ouyang Y (2013) A continuous approximation approach to competitive facility location design under facility disruption risks. *Transportation Res. Part B* 50:90–103.

Wentges P (1996) Accelerating Benders decomposition for the capacitated facility location problem. *Math. Methods Oper. Res.* 44: 267–290.

Xie F, Huang Y, Eksioglu SD (2014) Integrating multimodal transport into cellulosic biofuel supply chain design under feedstock seasonality with a case study based on California. *Bioresource Tech.* 152:15–23.

Xie W, Ouyang Y (2013) Dynamic planning of facility locations with benefits from multitype facility colocation. *Comput.-Aided Civil Infrastructure Engrg.* 28:666–678.

You F, Tao L, Graziano DJ, Snyder SW (2012) Optimal design of sustainable cellulosic biofuel supply chains: Multiobjective optimization coupled with life cycle assessment and input-output analysis. *AIChE J.* 58:1157–1180.

Zamboni A, Shah N, Bezzo F (2009) Spatially explicit static model for the strategic design of future bioethanol production systems. 1. Cost minimization. *Energy Fuels* 23:5121–5133.